Low temperature sintering of Gadolinium Doped Ceria Electrolyte

A dissertation submitted in fulfilment of the requirements for the Degree

of

MASTER OF SCIENCE
in
PHYSICS

Submitted by
Jahnvi Goyal

Roll No. 302104011

Under the Guidance of

Dr. Jayant Kolte

Asst. Professor, SPMS

2023

School of Physics and Materials Science

Thapar Institute of Engineering and Technology, Patiala

(Declared as deemed-to-be University)

Patiala, Punjab (India)

DECLARATION

I hereby declare that the work which is presented in dissertation entitled "**Low temperature sintering of Gadolinium Doped Ceria Electrolyte**" in partial fulfilment of the requirements for the award of the degree of Masters in Physics, School of Physics and Material Science, Thapar Institute of Engineering & Technology (Deemed to be University), is an authentic report of original work of mine carried out under the guidance of Dr. Jayant Kolte. It refers other's researcher's work which are duly listed in the reference section. The matter contained in this dissertation has not been submitted, neither in part not in full to any other degree to any other university or institute except as reported in text and references.

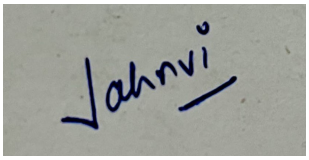

(Jahnvi Goyal)

Roll No.: 302104011

Place: Patiala, Punjab

Date: 16-08-2023

It is certified that the above statement made by the student is correct to the best of my knowledge and belief.

Date: 16-08-2023

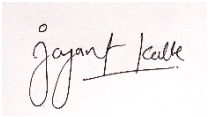

(Dr. Jayant Kolte)

Assistant Professor

School of Physics and Material Science,

Thapar Institute of Engineering & Technology, Patiala

CERTIFICATE

This is to certify that the present research work entitled "**Low temperature sintering of Gadolinium Doped Ceria Electrolyte**" which is being submitted by Jahnvi Goyal in fulfilment of the requirements for the award of the degree of Masters in Physics, School of Physics and Material Science, Thapar Institute of Science and Technology, Patiala is a record of bonafide research carried out by him under my supervision and guidance. The matter contained in this dissertation has not been submitted, neither in part not in full to any other university or institute for award of any degree.

Place: Patiala, Punjab

Date: 16-08-2023

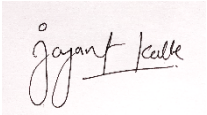

(Dr. Jayant Kolte)

Assistant Professor

ACKNOWLEDGEMENT

First of all, I would like to thank to the God, who is the creator of this universe and it is his mercy and blessing to me that this work become possible.

I would like to express my sincere gratitude to my supervisor Dr. Jayant Kolte for his unlimited guidance, insight and suggestions throughout the research. I thank him from the bottom of my heart for introducing me to the area of electro ceramics. I thank him for his great patience, constructive criticism and myriad useful suggestions apart from invaluable guidance to me.

I am grateful to Dr. Kulvir Singh, Head of School of Physics and Material science (SPMS) for his encouragement and help to carry out the thesis work.

I am also indebted to my senior research colleague Ms. Taranveer Kaur for her unconditional support and constant motivation whenever needed.

I am very grateful to my dear friends Jaffica, Pretty and Purujeet who has given me their friendship, put up with my odd hours, and provided me with lifts and practical help.

Last but not the least, I would like to thank my dear mother, my younger brother, without their support it was not possible to come so far.

JAHNVI GOYAL

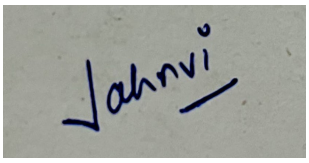

(302104011)

ABSTRACT

Gadolinium doped Ceria electrolytes has been considered as the most suitable materials for IT-SOFCs. In this study, the reduction in the sintering temperature has been done for the GDC doped samples. The effects of additions of Cu, Co and Bi oxide as sintering aids on $Gd_{0.1}Ce_{0.9}O_{1.95}$ has been studied. Powders of Gadolinium Doped Ceria with varying ratios of sintering aids was prepared and converted into pellets. These pellets were then sintered at various temperatures to ensure densification. The sintered GDC pellets with varying ratios of sintering aids were characterized through XRD, SEM and Impedance analysis. Density measurements were done and 3 wt% ratio of sintering aids shows the highest density. The XRD patterns show no secondary phases, which suggests that a single phase is formed in each sample. Also, the crystallite size decreases with increase in sintering aid concentration. From SEM images it is observed that the grain size has decreased considerably with respect to initial GDC sample without doping and dense microstructure was observed for 3 wt% samples. From the impedance analysis, high conductivities were obtained for Cu and Co doped GDC samples but conductivity decreases for Bi doped GDC samples than pure sample without addition of sintering aid. The conductivity follows the order: Bi< Cu< Co.

TABLE OF CONTENTS

LIST OF FIGURES

LIST OF TABLES

CHAPTER-1

INTRODUCTION

1.1 ENERGY CRISIS

Energy crisis is one of the major problems that we are facing nowadays. This is because of the energy consumption rate being much higher than the population growth rate and also due to our reliance on the non-renewable sources of energy. As clearly seen from Fig. 1.1 there is approximately 1.2 % increase in population whereas energy consumption rate is increased by approximately 1.9 %. Hence, this leads to more energy consumption than its production. This problem can be solved by using more renewable energy sources in the place of non- renewable sources of energy. Non- renewable energy sources cannot be used again and again and cannot be replenished e.g. coal, petrol, diesel, natural gas, etc.

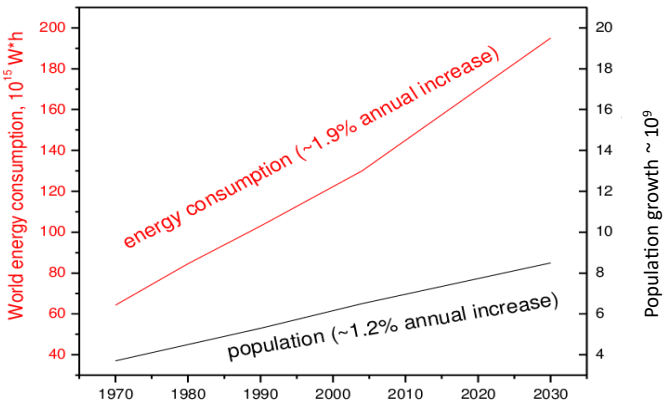

Fig. 1.1: Worldwide Energy Consumption and Population Growth, estimated from 1970-2030

Energy crisis can be resolved by substituting non- renewable energy sources with renewable energy sources, like wind and solar power. But the generation of renewable energy is sometimes unreliable, which is a significant obstacle to their widespread adoption. For instance, intermittent wind patterns allow for the generation of power during periods of low demand, such as the middle of the night, whereas wind patterns during periods of high demand may result in low levels of power production. So, we need an easy and reliable solution for the generation of electricity. One such solution is fuel cell. A fuel cell is a type of energy source having very good efficiency.

1.2 FUEL CELL

A fuel cell is an instrument which uses an electrochemical reaction to get electrical energy from chemical energy. Fuel cells operate similarly to batteries but in contrast to a battery, it needs an external fuel source. Although this increases the complexity of the system, it also significantly extends the amount of time that the cell can potentially run for, as removing the protracted recharge period that batteries have. In a manner similar to how batteries can be scaled, fuel cells may likewise be used for a wide range of power capacities, from small to large devices that produce power in MWs. However, some fuel cell systems, like SOFCs (Solid Oxide Fuel Cells), may potentially operate on a wide variety of fuels. This enables them to compensate the technology gap between hydrocarbon fuels. One of the key benefits of these devices is their high efficiency. They frequently achieve system efficiencies of over 70%, which makes them superior to other technologies like internal combustion engines (ICEs), which normally achieve peak efficiencies of only 35% [1]. Electrolyte, Cathode and Anode are the major components of fuel cell.

At the anode, a catalyst (such as fine platinum) oxidizes the fuel (often hydrogen) into a positively charged ion and negatively charged electron. The electrolyte allows the motion of ions through it but not electrons. Releases electrons then travel through a wire and an electric current is produced. The ions and electrons unite at the cathode and generates water or carbon dioxide.

The fuel cells can be connected in parallel to supply a larger current and in series to produce a higher voltage as needed to produce the desired amount of energy. This design is called fuel cell stack.

1.2.1 TYPES OF FUEL CELLS

Fuel cells are being developed in a variety of forms, each with unique features and applications. Classification of different fuel cells on the basis of electrolyte employed are discussed below in Table 1.1 [2]

Table 1-1 Types of fuel cells classified on the basis of electrolyte, charge carried in the electrolyte, operating temperature and efficiency:

Type	Electrolyte	Charge carried in the electrolyte	Operating Temp. (°C)	Efficiency
Polymer electrolyte fuel cell (PEFC)	Thin polymer electrolyte.	H^+	~90	40-50 %
Alkaline fuel cell (AFC)	Potassium hydroxide (KOH)	OH^-	60-250	50 %
Phosphoric Acid fuel cell (PAFC)	Phosphoric Acid	H^+	180-210	40 %
Molten Carbonate fuel cell (MCFC)	Alkali Carbonates	CO_3^{2-}	600-700	45-55 %
Solid Oxide fuel cell (SOFC)	Ceramic solid oxides	O^{2-}	800-1000	50-60 %

1.3 SOLID OXIDE FUEL CELLS (SOFCs)

Solid Oxide Fuel Cell (SOFC) uses an oxidation-reduction mechanism using oxygen ions to transform chemical energy from a fuel into electrical energy. Under ideal operating conditions, SOFCs can reach high energy conversion efficiency, often between 50% and 60%. They have a number of distinctive qualities that set them apart from other fuel cell types and function at high temperatures, often between 600 and 1000°C. SOFC is considered as a clean, dependable and sustainable energy source. It produces electric current by the chemical reaction between oxygen and hydrogen [3]. The following reaction occurs in the Solid Oxide Fuel Cells:

At Anode: $H_2 + O^{2-} \rightarrow H_2O + 2e^-$ Equation 1-1

At Cathode: $\frac{1}{2}O_2 + 2e^- \rightarrow O^{2-}$ Equation 1-2

Overall reaction: $H_2O + \frac{1}{2}O_2 \rightarrow H_2O$ Equation 1-3

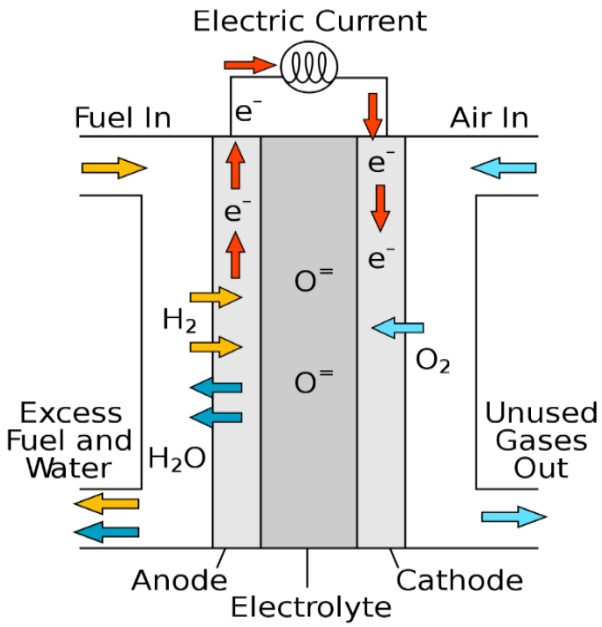

Fig. 1.2: A Schematic show working of a solid oxide fuel cell.

Fig. 1.2 represents the reactions occurring in a Solid Oxide Fuel Cell. The stacks of electrochemical cells that make up SOFCs are generally made up of membrane electrode assemblies (MEA). The MEA consists of porous anode, the porous cathode and dense electrolyte. SOFCs can be used both as stationary power generation and auxiliary power units in vehicles [4, 5]. Military sites, off-grid communities, and isolated locales can all benefit from SOFC electricity since they require consistent, dependable power.

1.4 COMPONENTS OF SOFCs

The electrolyte is a solid ceramic substance with a high conductivity for oxygen ions (O_2). Oxygen ions are permitted to move from the cathode to the anode by the electrolyte at the high working temperatures of SOFCs (usually 600–1000 °C). Oxygen in the atmosphere reacts with electrons and moves through the cathode to the surface of the electrolyte. Oxygen ions are produced on the anode side of the electrolyte. The gradient in oxygen partial pressure between the cathode and anode drives the transport of oxygen ions through the electrolyte. Fuel (hydrogen or hydrocarbons) is fed to the cell at the anode. In the case of hydrogen and hydrocarbons, a chemical reaction between the fuel molecules and oxygen ions (O^{2-}) from the electrolyte results in the production of water vapour and carbon dioxide, respectively. Heat and electrons are produced by the anode's electrochemical reaction. For practical purposes, the electrons are directed through the anode and external circuit. At the cathode, oxygen ions that goes through the electrolyte and electrons from the external circuit interact to form oxygen

ions. On the cathode surface, this process results in oxygen ions (O^{2-}). The cathode serves as the surface for the oxygen reduction reaction, which converts oxygen ions and electrons into oxygen molecules. The interconnect provides electrical connections between the fuel cells in a sequence and divides them into independent units inside the stack. It makes it easier for reactant gases (such as air and fuel) to move between nearby fuel cells. To resist the high-temperature environment and guarantee dependable electrical connections, the connecting material needs to have good electrical conductivity, chemical stability, and mechanical strength. The electrons produced at the anode are collected by the current collectors and sent to the external circuit. They also return the electrons from the external circuit to the cathode-electrolyte contact at the cathode. Typically, conductive materials such as metals are used to create the current collectors. [6]. The requirements of the cell components are:

- Microstructural stability and phase stability.
- Cell components compatibility with each other.
- Minimal thermal mismatch should be there between components.
- Chemical stability.

1.4.1 Cathode (LSCF-GDC)

The oxidising agent, usually oxygen from the air, is in direct contact with this, thus cathode must be stable in those conditions [1]. Doped La- manganite, which is a p-type semiconductor, is the cathode material utilised in SOFC systems the most frequently. Lower valent doping of $LaMnO_3$, because there is more Mn^{4+} in the material, cations improve electronic conductivity. Nano YSZ, $LaCoO_3$, GDC, Platinum electrodes and other materials had also been discovered to meet these requirements. $La_{1-x}Sr_xCo_{1-y}Fe_yO_{3-\delta}$ (LSCF, generally $x \sim 0.2$, $y \sim 0.8$) is considered superior to LSM and considered as a viable candidate for cathode material. LSCF (Lanthanum Strontium Cobalt Ferrite) possesses better chemical stability at high temperatures and under harsh operating conditions compared to LSM (Lanthanum Strontium Manganite). LSCF exhibits higher catalytic activity for the Oxygen Reduction Reaction, which is a crucial electrochemical reaction that occurs at the cathode in fuel cells. This means that LSCF can effectively facilitate the conversion of oxygen molecules to oxide ions, resulting in improved cell performance. The stability of the cathode material is vital for maintaining long-term cell performance and preventing degradation. LSCF has a lower polarization resistance, which refers to the resistance encountered by the flow of charged particles during electrochemical reactions. A lower polarization resistance leads to reduced voltage losses and improved power

density of the SOFC. LSCF exhibits good thermal compatibility with commonly used electrolyte materials, such as YSZ, which allows for better adhesion and compatibility between the cathode and electrolyte interfaces. This results in enhanced cell performance and reduced interfacial resistance. Also, it possesses higher ionic and electronic conductivity compared to LSM, enabling efficient transport of charge carriers within the cathode material. This promotes better electrode kinetics and enhances overall cell performance. But LSCF composites are used mainly as cathode materials as its ionic conductivity is low. Hence, LSCF composite is chosen as cathode material nowadays. In this study, we are using LSCF-GDC composite as cathode material.

1.4.2 Anode (NiO-GDC + sintering aid)

Usually, the fuel enters the cell through the anode layer. The fuel should be stable in severely reducing environment and offer little amount of ionic conduction so that ion transfer between anode and electrolyte takes place. It must also give some level of electronic conduction to allow the electrons to flow. Moreover, it must be chemically unrelated to the electrolyte substance. In addition, an anode must have thermal stability and sufficient mechanical strength to withstand physical weight and mechanical stress [7]. In order to improve processes occurring at the surface, it should also have catalytic activity [1]. Metals (Ni, Pt, Co and Ru) are employed as electrodes on the anode side where the environment is reducing. Due of its inexpensive price, Ni is the chosen option because of its low resistance to grain development and sintering. NiO is commonly used and considered superior to use as anode material as Carbon monoxide (CO) and hydrogen (H_2) gases, which are frequently utilised as fuel in SOFCs, can be oxidised by Nickel oxide with outstanding catalytic activity. Fuel is electrochemically oxidised by the anode, and NiO speeds up the reaction kinetics to make fuel conversion more effective. NiO is a semiconducting substance with an essential characteristic for the functioning of the anode that is, a fairly high electronic conductivity at elevated temperatures. This makes it possible for the fuel to transmit electrons to the anode-electrolyte contact efficiently, which is what causes electrochemical processes to take place. Nickel Oxide has strong thermal compatibility with various components of SOFCs, including the electrolyte and the cathode materials. This compatibility enhances stability of the Solid Oxide Fuel Cell and decrease thermal stresses. When compared to other materials, using anodes made of NiO can reduce polarisation losses. This is because its catalytic ability and electronic conductivity work together to enhance electrochemical performance and minimise overpotentials. Also, compared to certain other elements used in fuel cells, nickel is a plentiful and reasonably priced element. Due to this,

NiO is a viable option from the perspective of cost for SOFC production on a wide scale. But NiO composites are used mainly as anode materials as its ionic conductivity is low. Hence, NiO composite is chosen as cathode material nowadays. In this study, we are using NiO-GDC composite as cathode material.

1.4.3 Electrolyte (GDC+ sintering aid)

The electrolyte is positioned between anode and cathode in the Solid Oxide Fuel Cell system. It is used to conduct oxygen ions from cathode to anode. The anode or electrolyte usually constitutes a supporting structure for SOFC. In order to obtain good power densities, the electrolyte should have a conductivity of 0.1 S/ cm and 0.01 S/ cm for electrolyte and anode supported designs,respectively. As a result, choosing an electrolyte is subject to strict criteria. The electrolyte must possess the following properties in addition to its high conductivity [8]:

- Long-term mechanical strength,
- appropriate thermal expansion coefficient (TEC) compatible with both electrode material [7],
- long-term chemical stability,
- chemically inert toward both electrode material,
- ease of manufacture, and low cost

The well-known solid oxygen-ion conductors are largely composed of stabilised zirconia of the fluorite type, doped ceria, perovskite strontium/magnesium-doped lanthanum gallate (LSGM), and silicates and germanates of the apatite type [9, 10]. The most used electrolyte substance to date is zirconia stabilised with yttria at 8–10 mol%. The main benefits of YSZ are its pure ionic conductivity, excellent stability, good fracture toughness, and widespread availability [11, 12]. YSZ (Yttria stabilized Zirconia) operates at temperatures between 800-1000℃. The material's fundamental flaw is that it has minimal conductivity at intermediate temperatures. Below 800℃ its conductivity decreases substantially and therefore, Cerium oxide has been used as an electrolyte material due to high ionic conductivity than YSZ at low temperature. Doped bismuth [13] and doped ceria [14] have also produced conductivities that are higher. Nonetheless, undesirable electrical conduction would result from the lowering of Ce^{4+} and Bi^{3+} to Ce^{3+} and Bi^{2+} at reduced oxygen partial pressure. Conductivity of Gadolinium Doped Ceria is around 0.01 S/cm at 600℃ [15]. Also, the electronic conductivity of Gadolinium Doped Ceria is negligible at this temperature.

1.5 SINTERING

Sintering refers to a mechanism of forming a solid mass of material. It is done under pressure and heat without melting the material to its extent of liquefication. This phenomenon corresponds to diffusion of atoms in the material across particle boundaries and combine to produce a single mass. Ceramics, polymers, etc. are some of the examples of materials that follows this mechanism [16]. The particles are compacted into a "green body" before being sintered. About 55% of the green body's constituents are hard material particles (binding metals), 30% are lubricants, and 5% are pores [17]. To obtain a solid/compact body, the pores must be closed. Sintering is done to increase strength of the material and enhances the overall quality of the material.

1.5.1 LIQUID PHASE SINTERING (LPS)

Liquid phase sintering is used to form multi-phase, high performance components from powders. This process is used for the materials that are not easy to sinter. Fig. 1.3 shows the proper step by step mechanism of Liquid Phase Sintering. In LPS, an additive is added to the powder which will be sintered. The additive melts and pull the liquid into the pores. A favourable grain packing arrangement results from the liquid melting and entering the pores. The LPS mechanism is used in a variety of alloys and composites that melt at various temperatures. In this process, solid grains and a wetting liquid coexist while being sintered [16]. In the body being sintered, capillary forces act as a contraction, and there are numerous hard substance particle dissolution reactions in the melt [17]. For Metal Matrix Composites to sinter quickly, there must be a sufficient fraction of liquid binder. Essentially, the amount of liquid phase is managed by [18]:

- the eutectic point's coordinates in the quasi-binary system
- the actual sintering temperature, and
- the initial makeup of the powder mixture.

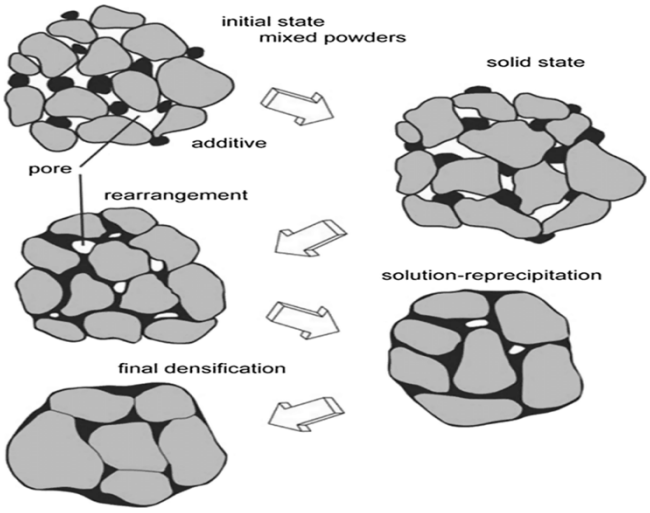

Fig. 1.3: Changes in the microstructure during Liquid Phase Sintering.

There are typically three processes involved in the liquid phase sintering process:

1. Heating that is non-isothermal; this method does not use pressing agents to bring powder particles into contact.
2. Isothermal stay at sintering temperature, when the binding phase melts and the sintering reactions are sped up by the influence of the liquid phase. Because the pores are closed off, the liquid phase densifies the body.
3. Allowing to reach ambient temperature.

Densification is ensured through the high temperature that softens the solid. The several phases in the sintering process cause a shrinkage, typically 18 to 20%. To obtain the right dimensions for the finished product, it is crucial to take shrinkage behaviour into account.

CHAPTER-2

LITERATURE REVIEW

2.1 Introduction

According to reports, materials based on GDC ($Ce_{1-y}Gd_yO_{2-\delta}$) are recently the best suitable electrolyte materials for Intermediate Temperature SOFCs because the chemical structure must be stable in both oxidizing and reducing atmosphere, it must also have the best possible physical characteristics (thermal expansion rate, mechanical strength, etc.). The fluorite structure of Cerium Oxide based materials has a face-centered cubic structure of cation and anion that occupies the tetrahedral voids. Pure CeO_2 does not contain enough oxygen vacancies to produce high ionic conductivity; as a result, acceptor cations like Gd^{3+}, Sm^{3+}, or Y^{3+} are used to substitute host Ce^{4+} in order to inject oxygen vacancies into the structure. But the major drawback is that these materials have poor sinterability. Several researchers have suggested that to lower the sintering temperature of CeO_2- based materials, small amounts of additives such as Mn, Co, Cu, Bi, Li and Fe are introduced that are able to enhance the sintering performance of the material [19]. The aim of this work focuses on observing the impact of adding different sintering aids (Cu, Co, Bi) on the thermal, electrical and chemical properties of $Ce_{0.8}Gd_{0.2}O_{2-\delta}$.

2.2 Densification of GDC using sintering aids

Synthesis of dense electrolyte layer is important as the residual pores may allow the gas to leak or short-circuiting the cell. The sintering density of GDC can be enhanced by decreasing the particle size to a nanoscale or by using sintering aids. In this study, focuses on how to improve the densification of GDC at lower temperatures by using sintering aids such as Bi, Co, Cu [20]. Addition of these dopants along with reducing particle size can lower the sintering temperature. These metal oxides reduce the sintering temperature by allowing liquid phase sintering of the electrolyte, thus allowing the sintering at less than 1200 °C. In liquid phase sintering, the additive melts initially wetting the solid and then allows the sintering of the solid by providing capillary action which allows the rearrangement of grains. This rearrangement reduces the porosity and produces very dense solid at comparatively low temperatures [21].

Nicholas et al. [22] in their study found that dopants such as Cu, Co and Mn etc. reduce its sintering temperature, whereas Ca, Mg, and Ni have negligible effect. They used Vegard's slope method to find the solubility of these ions in cerium oxide. If r_i is the difference between the

ionic radii of the dopant and Ce^{4+} and z_i is the difference in the charge between the dopant and Ce^{4+}, then the Vegard's slope (X) is given by

$$X = 0.22r_i + 0.00015z_i \quad (5)$$

The additives with absolute value of X >> 0 induces LPS in GDC while those having moderate values have no effect. On the other hand, Al and K having very large value of |X| increase the sintering temperature of GDC-10 as they may form a second phase which inhibits the liquid sintering and forces the material to undergo solid sintering.

E. Yu. Pikalova et al. [19] studies how Co, Mn, Ti and Fe oxide additions affect the sinterability of $Ce_{0.8}Gd_{0.2}O_{2-\delta}$ as well as its crystal-chemical, electrical and thermal properties. Whether they were added before or after synthesis, the results show that these oxides improve the mixed oxide's sinterability. The Co_2O_3 is the most effective sintering aid. In space group Fm3m, lattice parameters of Cerium Gadolinium Oxide samples with 1 mol% of various metal oxide are enhanced. The sample's linear thermal expansion coefficients are calculated using the thermal expansion data dependent on temperature. The electrical conductivity of pure GDC is decreased by manganese oxide additions, however it is increased in the following sequence by the other dopants: Ti, Fe, and Co.

Roy et al. [23] have investigated the impact of Sr doping on the densification and ionic conductivity of GDC. Dilatometric measurements of Strontium doped Gadolinium Doped Ceria and green sample of undoped Gadolinium Doped Ceria are done to examine the sintering temperature regimes and the sintering nature. The X-ray diffraction pattern is used to study the sintered sample's cubic crystal structure. Ionic conductivity of (Sr-GDC), which is 0.072 S/cm, has increased significantly by twofold when compared to GDC (0.028 S/cm), as shown by microstructural study. This rise in overall conductivity may be the result of improved densification and larger grains. Increased oxygen ion mobility and decreased lattice binding energy result from strontium doping, which also lowers activation energy.

S. Taub et al. [24] investigate the variation of electrical properties of GDC with the addition of Cr or Co (transition metals) dopants. Co and Cr, used as an effective sintering agent, will increase the density of the Gadolinium Doped Ceria electrolyte. Following sintering, these transition metals are isolated at triple grain junctions and at grain boundaries where second phase precipitates. With a 2% incorporation of Co, intrinsic conductivity of the grain boundaries rises, whereas even a small concentration of Cr causes the intrinsic conductivity of

the grain boundaries to fall. Therefore, it has been discovered that the change in conductivity is minimal for these dopants.

Dasari et. al. [25] offered a better approach to considerably lower this temperature to 600°C. GDC nano crystal was created using the co-precipitation process. Lithium (Li) is utilized as a supplementary dopant during liquid phase sintering. In the electrolyte material produced by microwave sintering, the sintering temperature was reduced significantly to 600° C. SEM/TEM micrographs clearly illustrate the enormous expansion in grain-size of Lithium doped GDC sample (150 nm) as compared to GDC sample (30 nm). At 600 °C, Li-GDC has conductivity 1.00×10^{-2} S cm^{-1} and its activation energy is 0.53 eV.

M. Biesuz et al. [26] studies that it is possible to create 10 mol% Gd-doped cerium oxide via co-precipitation, which is stable over a wide range of temperature, partially crystallised, partially amorphous, and exhibits low levels of hydration. This behaviour differs somewhat from that of other ceramic systems, including precipitates made of zirconia. DTA-TG, XRD, TEM and nitrogen adsorption studies were done to characterise co-precipitate. Nano-powder is performed during both normal and flash sintering. The traditional sintering cycle generated a material with uneven sub-micrometric grain size, whereas flash sintering allowed development of a material that was precisely densified. Very dense GDC electrolyte can be formed within few minutes.

G. Accardo et al. [20] studies that the use of lithium as sintering aid in GDC can bring down the sintering temperature (T_s) to as low as 800 °C. Scanning Electron Microscopy, XRD, BET analysis, FTIR spectroscopy and electrochemical impedance spectroscopy characterization techniques were used. At sintering temperature of 1250°C the densification was found to be >97% of the theoretical density and at 1500°C it is >99%, by addition of 2 mol% of Li. The lithium substitution should be limited to small amounts as higher quantities may form a lithium oxide layer at the grain boundaries, that may inhibit the ion conduction. Li-doped pellets sintered at a temperature of 1250 °C have an ionic conductivity with highest value of 5.2×10^{-2} S cm^{-1} at 800 °C, the same as pure pellets at 1500°C. It is found that for achieving high conductivity values and to lower the sintering temperature, lithium doping serves as a very effective technique.

Valdebenito et al. [27] have suggested that by using a precise electric field, the temperature needed to sinter GDC-10 made via tape-casting can be greatly lowered. He has flash sintered the GDC fabricated by tape casting at 445 °C under the influence of electric field of 170 V/cm.

With a constant electric field, the density of the electrolyte increased with increasing current density.

S.M. Jamil et. al. [28] conducted research to determine the efficiency of nano-sized GDC particles in producing thick GDC electrolytes at low sintering temperatures. Sintering temperature reduction will have a significant positive impact on SOFC fabrication. Using a phase inversion approach, a doped solution with a 30% nano-sized loading was created and cast in the form of a flat sheet. The mechanical strength, morphology, and surface roughness of this sheet are tested. Electrolyte/anode DLHFs half-cells for micro-tubular solid oxide fuel cells were constructed using the Phase inversion-based co-extrusion/co-sintering process, and then they underwent morphological and gas fitness tests. The results showed that development of the dense and gas-tight CGO layer is induced by 30% nanoparticle sintered at 1450° C. Using H_2 as the fuel results in power density of 0.66 W cm^{-2}. One of the main issues with SOFCs is their inability to adequately densify the electrolyte material because to the high temperature (>1300°C) necessary for sintering.

L. Spiridigliozzi et al. [29] successfully employs flash sintering technique to GDC. In flash sintering, GDC can be sintered at 600 °C temperatures. Surprisingly, the densification is not enhanced by the use of Li_2O and CoO as sintering aids. At temperatures just around 600 °C, highly dense (approx. 99%) GDC-10 materials with grains of roughly 200–300 nm may be produced through flash-sintering. At 600 °C, total conductivity is found to be 1.13x 10^{-2} S/cm, which is equivalent to the value observed on samples that were traditionally sintered at 1500 °C. There is no need to use any sintering aid since their use will only inhibit the process.

G. Accardo et al. [30] proposes that the materials doped with 1–5 wt% oxides of Bi have been effectively created using sol-gel combustion synthesis technique to enhance the microstructural and electrochemical properties of GDC electrolytes. Sol-gel combustion makes it easier to replace the massive Bi^{3+} cations and mix the precursor molecules molecularly, which significantly lowers the sintering temperature. The GDC densification rises to above 99.7% with the use of Bi_2O_3 as a dopant, and its typical sintering temperature is lowered by 300 °C.

G. Accardo et al. [31] suggests that for doped ceria ceramics to be effectively used as electrolytes for industrial-scale IT-SOFCs, the sintering temperature must be lowered. In following work, the sintering aid for 20 mol%(Gd) -doped ceria was Bi (0.5 and 2 mol%). Bi/Gd co-doped ceria nano-powders were easily made using a quick and low-cost sol-gel combustion synthesis. The resulting powders had excellent electrochemical and high

sinterability characteristics. Even after prolonged thermal treatments at 700°C there are no structural changes observed in the Bi doped GDC.

P. Mangifesta et al. [32] explores that one of the most suitable electrolytes for intermediate temperature SOFC is $Ce_{0.8}Gd_{0.2}O_{2-\delta}$ (GDC). One of the biggest obstacles to producing totally dense electrolyte is lowering the sintering temperature. The morphological properties of the original powders have a substantial influence on the sintering activity of a ceramic material body, and the existence of a sintering aid can also have an impact. There are numerous ways to incorporate the latter into the main phase, with ball milling and precipitation being the two most popular. Using nitrate salt and ball milling, GDC powders with various specific surface areas were doped by 3mol% copper oxide before being sintered and then measured for dilatometry. The findings show that the ratio has a significant impact on the sintering between specific surface area of CuO and pure GDC. Surprisingly, it was discovered that ball milling was the most efficient doping process for CuO-doped GDC, producing a thick electrolyte at temperatures as low as 900°C.

M. Biesuz et al. [33] studies and suggests that some other methods are also used for sintering GDC electrolyte at lower temperatures for shorter time periods such as flash sintering. In flash sintering an electric field is applied along with simultaneous heating in the furnace. The current is then forced to pass through the sample and at a particular onset temperature, material densifies rapidly in very short time. It represents an effective way to lower the financial, energy-related, and environmental consequences of firing through sintering. Furthermore, it enables the emergence of unusual and non-equilibrium microstructures.

G. Accardo et al. [34] explores that by 2–5 mol% of lithium doping, lithium-gadolinium-doped ceria electrolytes are created. The inclusion of lithium lowers the sintering temperature to 950 °C. It has been observed that the electrochemical characteristics are far superior than those of pure GDC. Adding 3 mol% of lithium results in a maximum total conductivity of 3.59 $x10^{-2}$ to 1.41 $x10^{-1}$ S cm^{-1} at the middle of the operating temperature range. The next step is to construct and test an electrolyte-supported SOFC under various gaseous atmosphere and operating temps. The maximal power density (at 668 mA/cm^2) and 750 °C) is 359 mW/cm^2. The outcomes show the viability of both the synthesis cycle and electrolyte fabrication for use in industries, as well as the dependability and utility of developing a competitively priced fuel cell system.

G. Accardo et al. [35] studies that GDC co-doped electrolytes were created using a quick, single step sol gel combustion synthesis process. Using this process, Li and Co oxides (0.5- 2%) were produced to enhance properties of GDC. The solubility of the dopant and the behavior of the sintering were predicted using Vegard's slope theory. The GDC become much dense than previous and its usual sintering temperature is lowered to 1000–1100 °C with lithium and cobalt precursors as a dopant, improving its electrochemical characteristics. According to impedance studies, high total conductivities of $1.26x10^{-1}$ S cm^{-1} and $8.72x10^{-2}$ S cm^{-1} at 800 °C were achieved for 2 mol% Li and 0.5 mol% Co, respectively.

Grilo et. al. [36] used Lithium and Sodium carbonates as sintering aid in GDC. A dense electrolyte with > 95% density is obtained at sintering temperature of 1100 °C for 4 h. Alkali salt eutectic mixtures have been confirmed as promising sintering aids because the overall electrical characteristic on their addition shows that the results are only marginally different than reference GDC.

Table 2-1 shows the effect of different sintering aids and methods on the sintering temperature (T_s), density and conductivity of GDC.

Table 2-1 Effect of sintering aids on the density and conductivity of GDC

Sintering aids / Sintering method	**T_s (°C)**	**Density (%)**	**σ (S/cm)**	**References**
Li	1250 1500	>97 >99	5.20×10^{-2}(800 °C)	[20]
	950	>98	3.59×10^{-2}(600 °C)	[34]
	600		1.00×10^{-2}(600 °C)	[25]
	1000	~99	1.26×10^{-1}(800 °C)	[35]
Bi	1200	>99	3.10×10^{-2}(600 °C)	[30]
	1250	~96	1.99×10^{-2}(600 °C)	[31]
Co	1150 1200	91 93		
	1100	>97	8.72×10^{-2}(800 °C)	[35]
Fe	1000	>95	3.80×10^{-2}(800 °C)	[37]
Flash sintering	600	~99	1.13×10^{-2}(600 °C)	[29]

D. Guctas et al. [38] suggests that by using the cellulose templating (CT) and PVA templating (PVAT) procedures, $Sm_{0.2}Ce_{0.8}O_{1.9}$ (SDC20) electrolytes were created, and they were then examined using TGA/DTA, XRD, EIS, and SEM analyses. After calcining at 600 °C, SDC20 powders with a single fluorite phase were produced. The CIP method was used to manufacture the pellets, which were then sintered for various lengths of time at temperatures between 1200 and 1400 °C. Using the CIP method, pellets were made and sintered at the 1200–1400 °C temperature range for 5, 1, and 6 hours, respectively. All samples obtained a relative density of more than 88%. SEM pictures are used to analyse the grain growth kinetics. Using the linear intercept approach, the average grain sizes were calculated. that which is dominant. The activation energy of the sintering was estimated once the process, grain boundary diffusion, was identified. The sample with the highest ionic conductivity (0.050 S cm^{-1}) was sintered at 1400 °C. As it produces higher performance electrolytes, the cellulose templating method is more efficient than the precipitation and solid-state methods at creating mixed oxide structures.

CHAPTER-3

EXPERIMENTAL DETAILS

3.1 Preparation of electrolyte material (GDC + sintering aid)

Fig. 3.1 represents the flow of synthesis of electrolyte material. Commercially available powder of Gadolinium Doped Ceria ($Gd_{0.1}Ce_{0.9}O_{1.95}$) (Fuel Cell materials, USA) with sintering aids (CuO, Loba- Chemie), (Bi_2O_3, Alfa Aesar), (Co_3O_4, Sigma Aldrich) were used as electrolyte materials. The sintering aid powder was prepared by adding various ratios of sintering aid and GDC powder. Five samples with each sintering aid were prepared and the densification occurred due to it was observed. Here, addition of 1-5 wt % sintering aids with 99-95 wt % GDC powder were made, respectively. Both powders (GDC+ sintering aid) were dissolved in ethanol. The molar ratio of the sintering aid powder (GDC+ sintering aid) and the ethanol and that of zirconia balls and sintering aid powder was chosen as 2:1. The samples are then put on a rolling mill overnight to ensure proper mixing. After that, the solution is kept in oven at 65-70°C for drying and were grounded into the fine powder by using agate mortar and pestle. The dried powders are then converted into pellets and then sintered at various temperatures. The sintered pellets are then subjected to density measurements to ensure proper densification required for the electrolyte material.

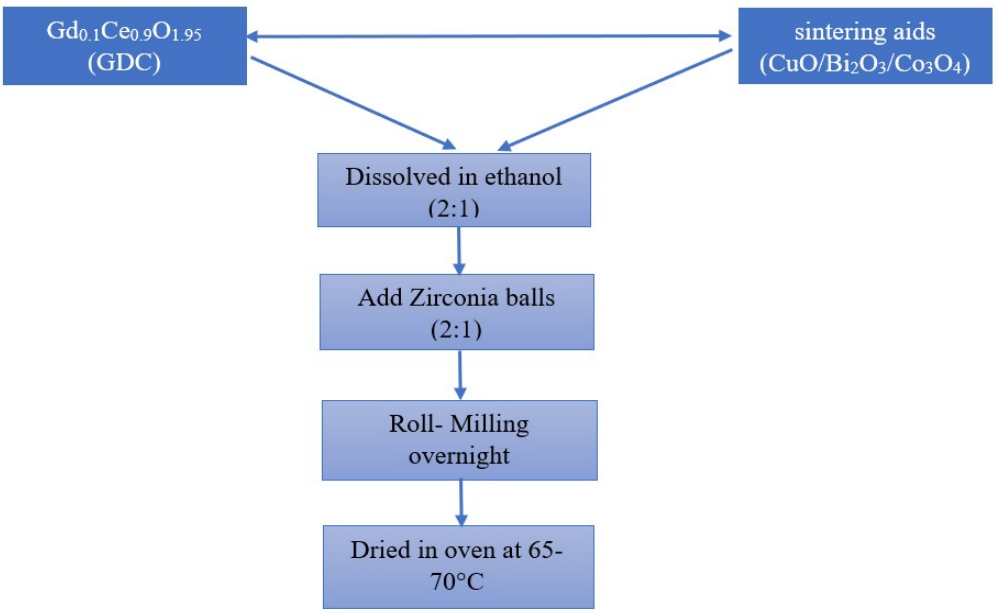

Fig. 3.1: Flowchart of synthesis of electrolyte material.

3.2 Pellet formation

Pellets are formed in die of diameter 10 mm. In this work, the amount of powder for forming each pellet is taken as 0.5 g. Thus, with die of diameter 10 mm and 0.5 g powder, pellets of thickness >1 mm are made. Pellets of (1-5) wt.% powder of Copper Oxide (CuO), (1-5) wt.% powder of Cobalt Oxide (Co_3O_4), (1-5) wt.% powder of Bismuth Oxide (Bi_2O_3) are fabricated in hydraulic pellet press. The weight of the powdered sample is measured precisely upto three decimal places. Sample powder is then placed in die of 10mm diameter and by un-axial compression, pellets of desired thickness are obtained in hydraulic pellet press. Pressure of 10 kg/cm^2 is applied to hydraulic pellet press to form pellets. The pellets thus formed having different weight percentages of sintering aids (1-5 wt.%) are then sintered at various temperatures to optimize for required high densities. In this section, pellets are sintered at temperatures 900°C, 1000°C, 1100°C and 1200°C (selected through melting points of sintering aids) for 4 hrs with heating rate 5°C/ min. During sintering, a layer of commercially available powder of GDC (GDC-10) is kept under the pellets in crucibles to avoid chemical reactions. Several pellets are made to sinter at these temperatures to ensure densification and their densities are calculated.

3.3 Density measurements

After sintering of pellets at various temperatures, the density calculations of the sintered pellets are done. Before taking density measurements, the pellets are polished by different grates of emery paper (600, 800, 1000, 1200) to ensure the removal of extra powder that sometimes stick to the surface of the pellet during sintering. The grounded pellets are then sonicated at room temperature for 2-3 mins. Polishing and sonication are very important for accurate measurements of density. The theoretical density of a composite(GDC) is calculated by the following formula [38]:

$$\rho_{(th)} = \frac{4}{N_A a^3}\left[xM_{Ce} + (1-x)M_{Gd} + (2-x)M_o\right] \qquad \text{Equation 3-1}$$

where, x is the concentration of Ceria, M_{Ce} is the molecular weight of Ceria,

M_{Gd} is the molecular weight of the commercial powder of GDC, M_O is the molecular weight of the oxygen, N_A is the Avogadro number, and a is the lattice parameter.

All the required quantities in the above formula are calculated and substituted in above equation to obtain the theoretical density of the pellets. The theoretical density of GDC is found to be 7.21g/cm^3 and all the calculations were done w.r.t this theoretical density.

For calculation of experimental density ($\rho_{(exp)}$), Archimedes principle is used. According to Archimedes principle, density is given by Equation 3-2:

$$\rho_{(exp)} = \frac{W_a}{W_a - W_w} \text{ x } \rho_w \qquad \text{Equation 3-2}$$

where, $\rho_{(exp)}$ is the experimental density, w_a is the weight of pellet in air, w_w is the weight of pellet in water, and ρ_w is the density of water.

After that relative density is obtained from the Equation 3-3:

$$\rho_{(rel)} = \frac{\rho(exp)}{\rho(th)} \text{ x } 100 \qquad \text{Equation 3-3}$$

After obtaining relative density measurements, a temperature value (from 900°C, 1000°C, 1100°C, 1200°C) is selected at which characterizations are performed.

3.4 Phase Analysis

XRD technique was applied to the samples to observe the crystalline structure. It is useful for researching atomic spacing, structures of crystals, crystallite sizes, lattice parameters and phase analysis of the material. These all are helpful in understanding the composition and characteristics of synthesised materials.

The constructive interference of the crystalline sample with the monochromatic X-rays is entirely responsible for the diffraction. A cathode ray tube emits X-rays when an electron with sufficient energy ejects electrons from the target material's inner shell, creating characteristic X-ray spectra. Copper having CuK_α wavelength value of 1.5418 Å is the most often used target material. Collimated X-rays are focused and directed at the specified sample. The sample meets the requirements of Bragg's law ($n\lambda = 2d\sin\theta$), and there is constructive interference takes place. After diffraction, the rays are found, examined, and finally counted. After scanning the material, the diffraction patterns are acquired at a range of 2θ angles [39].

X- Ray diffraction analysis was done on powdered samples using SmartLab SE (Rigaku) with CuKα radiation in scanning range of 2θ = 20°– 90° and a step size of 0.01°.

Fig. 3.2: Smart lab SE (Rigaku) setup for XRD.

The lattice parameter ‘a’ is given by the following equation,

$$d = \frac{a}{\sqrt{h^2 + k^2 + l^2}} \qquad \text{Equation 3-4}$$

where, a is the lattice parameter, (hkl) are the miller indices values of the crystalline planes and d is the interatomic spacing.

Crystallite size ‘d’ of the samples is obtained by using Scherrer equation [40]:

$$d = \frac{k\lambda}{\beta cos\theta} \qquad \text{Equation 3-5}$$

where, k is a constant, λ is the wavelength of X- ray beam used, β is Full Width at Half Maximum width, and θ is the diffraction angle.

3.5 Microstructure Analysis

The scanning electron microscope (SEM) is the best suited method to examine the sample's microstructure. The basic components of a SEM include an electron column, scanning systems, detectors, a vacuum system, and electronic controllers. The electron gun generates a high energy electron beam, which is subsequently brought into focus on the specimen by electron lenses. When an accelerated electron strikes a specimen surface, electromagnetic radiation is

released. This radiation is utilized to evaluate structural elements and image formation. The detector gathers up three different types of electrons: first, back scattered electrons that have changed direction; second, electrons that have not undergone a change in kinetic energy; and third, electrons that undergo inelastic scattering, which causes them to transfer some of their kinetic energy to the target electron and reduce its kinetic energy. Signals are gathered by the detector, amplified, and presented on the monitor [41].

Here, microstructural properties of the sintered pellets were examined via Scanning Electron Microscope (Carl Zeiss Sigma 500 FEG-SEM) in secondary emission mode. Fig. 3.3 represents the Carl Zeiss Sigma 500 FEG-SEM setup for SEM analysis. The images obtained from SEM are then analyzed to check the density in the sample. Grain size is found via ImageJ software.

Fig. 3.3: Carl Zeiss Sigma 500 FEG-SEM setup for microstructure observation.

3.6 Impedance Analysis

Conductivity measurements of the sintered pellets are done by Ametek 1260A Impedance/ Gain- Phase analyzer at 0.1 V_{rms} in the temperature range 100°C- 600°C. These measurements are performed in frequency range of 10 Hz- 1 MHz. Fig. 3.4 represents Ametek 1260A Impedance/ Gain- Phase analyzer setup for performing conductivity measurements.

Fig. 3.4: Ametek 1260A Impedance analyzer.

To perform electrical measurements, the sintered pellets are first polished and then silver paint is applied on both the sides of sintered pellets. The pellets with silver paint are baked at 400°C for 30 mins. At 400°C, the organic components in the silver paste were burned out, resulting in the consolidation of electrodes with very low contacting resistance.

In a polycrystalline electrolyte, the observed impedance spectra are influenced by both grain inner and grain boundary conduction [8].Value of the equivalent circuit can be used to fit both capacitance and resistance.

The grain inner conductivity is given as, $\sigma_{gi} = \frac{L}{R_{gi}A}$

And, the grain boundary conductivity can be expressed as, $\sigma_{gb} = \frac{L}{R_{gb}A}$

where, R_{gi} is the grain inner resistance, R_{gb} is the grain boundary resistance, A is cross- sectional area and L is thickness of sample.

The total resistance R_T is given by, $R_T = R_{gi} + R_{gb}$

The total conductivity 'σ_T' thus becomes,

$$\frac{1}{\sigma T} = \frac{1}{R_T} \qquad \text{Equation 3-6}$$

The slope of linear fits of the Arrhenius plots of total conductivity gives the value of activation energy.

$$\sigma_T = \sigma_0 \exp\left(\frac{-E_a}{kT}\right) \qquad \text{Equation 3-7}$$

where, σ_T is the total conductivity, σ_0 is the pre-exponential factor, k is the Boltzmann constant, E_a is the activation energy.

The Arrhenius plot for the calculation of total conductivity and activation is given below (Fig. 3.5)

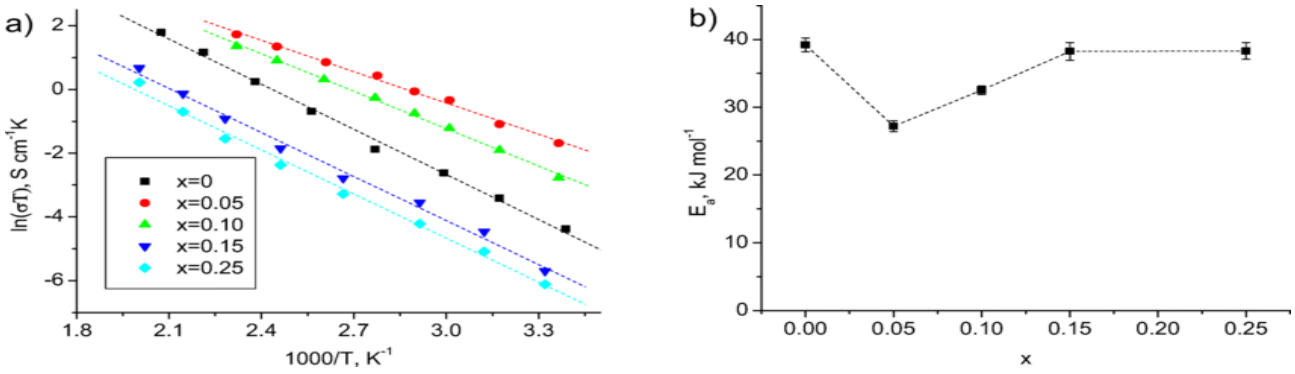

Fig. 3.5: (a) Arrhenius plots for total conductivity and (b) activation energy [42]

3.7 Binder Solution Preparation (PVA)

For anode tape casting, Polyvinyl Alcohol (PVA) is used as binder. The binder solution of PVA is prepared for anode fabrication. PVA solution is made by adding 6.2 wt.% of PVA to distilled water, for example, 1.5 g of PVA powder in 10 ml of water for a 15 wt.% solution. Then the PVA solution is kept in refrigerator for cooling for nearly 1 hour. After that the binder solution is kept on a hot plate and a magnetic stirrer is used to stir the solution continuously. The mixture should be constantly stirred until it became transparent. Temperature can be set to 130 °C to ensure that PVA dissolves quickly in distilled water. A cone-shaped shape must arise in the beaker while spinning to ensure that PVA and distilled water are mixed uniformly. The solution must stir until a clear solution of PVA is formed (approx. 30-40 mins). And then this solution is kept for cooling at room temperature and then used in anode fabrication.

3.8 Anode Tape Casting

NiO-GDC with sintering aid (CuO, Co_3O_4, Bi_2O_3) were selected as anode materials. For anode, 65 wt % Nickel Oxide (NiO) and Commercially available GDC powder (35 wt %) were doped with 3 wt % prepared powders of each sintering aid. In this study, we made anode tapes of NiO-GDC (65:35) with prepared CuO (3 wt %) powder, NiO-GDC (65:35) with prepared Co_3O_4 (3 wt %) powder, NiO-GDC (65:35) with prepared Bi_2O_3 (3 wt %) powder. They were mixed with DI water and dispersant Darvan C-N (6 wt %) and put on rolling mill overnight. Then, octanol (defoamer) and plasticizers such as Glycerol (3.9 wt %) PEG (Polyethylene Glycol) (3.9 wt %) were added and then again kept on rolling mill for about 3 hours. After that PVA (6.2 wt %, as 15% solution in water) is added to the tape slurry and placed on roll mill.

After 1 hour of mixing, the tape slurry was casted using Doctor's blade with tape thickness of 30 μm on a Mylar Film. The casted tapes were put in refrigerator for drying for about 24 hours.

3.9 Electrolyte Spray Coating

Spray coating of the electrolyte was done on the tapes prepared. The spray slurry was prepared by mixing commercial GDC powder and prepared 3 wt % powder of each sintering aid ((CuO, Co_3O_4, Bi_2O_3) (55 wt %), Darvan C-N dispersant (6 wt %) and DI water (22 wt %) and then placed on rolling mill for mixing. After mixing overnight, Polyethylene Glycol (PEG, 3.8 wt %) and binder solution of Polyvinyl Alcohol (PVA, 13.2 wt %) were added to the electrolyte slurry and again kept on rolling mill. The spray was then done on the tapes (anodes) fabricated through tape casting after about 3-4 hours of mixing. For accuracy, the electrolyte film should be denser and thus, to ensure densification the film was pressed in hydraulic pellet press. The prepared samples of the anode tapes and sprayed electrolyte films were then sintered at 1000 °C for 6 hours.

3.10 Cathode Brush painting

After co-sintering of the electrolyte film and the anode tape, cathode paint was applied on the sintered samples. LSCF-GDC (65:35) was selected as cathode materials. A solution mixture of Ethyl cellulose (10 %) and terpineol (90 %) was prepared using a magnetic stirrer which is used as a solvent. The cathode slurry for cathode ink painting was prepared by adding commercial Gadolinium Doped Ceria Powder $Gd_{0.1}Ce_{0.9}O_{1.90}$ and $La_{0.8}Sr_{0.2}Co_{0.8}Fe_{0.2}O_{2-\delta}$ (LSCF-GDC, 65:35) with prepared ethyl cellulose and terpineol in agate- mortar. In this study, cathode ink is prepared by mixing 1g of LSCF-GDC prepared powder with 1 ml of prepared solvent solution (ethyl cellulose + terpineol). The cathode ink was then applied on the electrolyte side of the sintered samples and kept in oven for drying at 70-75 °C. This process was repeated four times and thus four layers of the cathode ink were applied and then sintered at 1000 °C for 2 hrs in the furnace. After sintering, silver paint is applied on both sides of the samples for current collection and baked at 400°C for 1 hr.

Thus, the final cells are fabricated by using the above process.

CHAPTER-4

RESULTS AND DISCUSSIONS

4.1 Density measurements

Density is measured for all the samples i.e Cu- doped GDC, Co- doped GDC and Bi- doped GDC with varying ratios (1-5 wt %) through Archimedes principle. It was observed that the samples with 3 wt% addition of sintering aid has highest density. Cu- 3 wt%, Co- 3 wt% and Bi- 3 wt% possesses densities 97.3%, 95.5% and 94.5% respectively. The densities of all the samples with varying ratios of sintering aids is represented in Fig. 4.1:

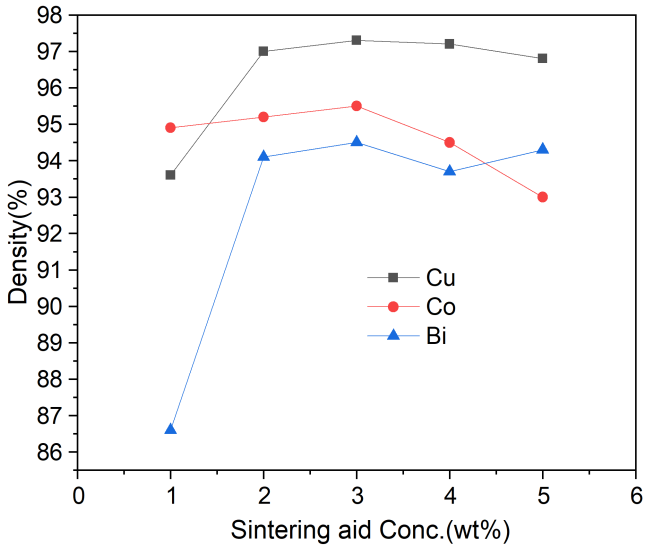

Fig. 4.1: Density of sintered samples of Cu, Co, Bi with sintering aid measured by Archimedes principle.

4.2 X-Ray Diffraction Analysis

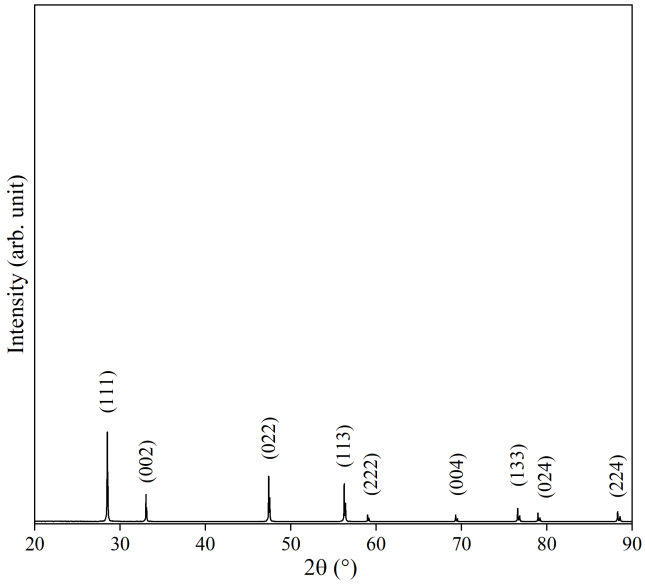

Fig. 4.2: XRD pattern of GDC at 1450°C.

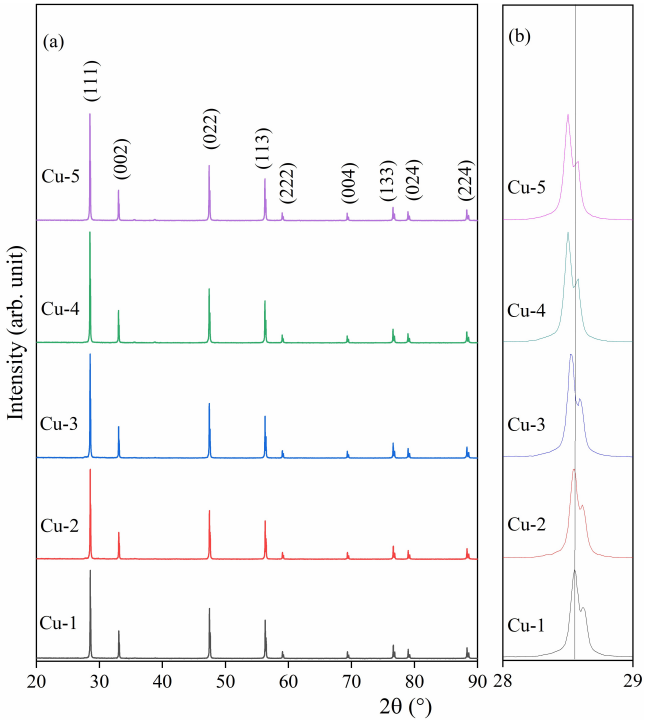

Fig. 4.3: (a) XRD pattern of Cu-doped GDC powders (1-5 wt %) sintered at 1000°C (b) enlarged view of the (111) peak.

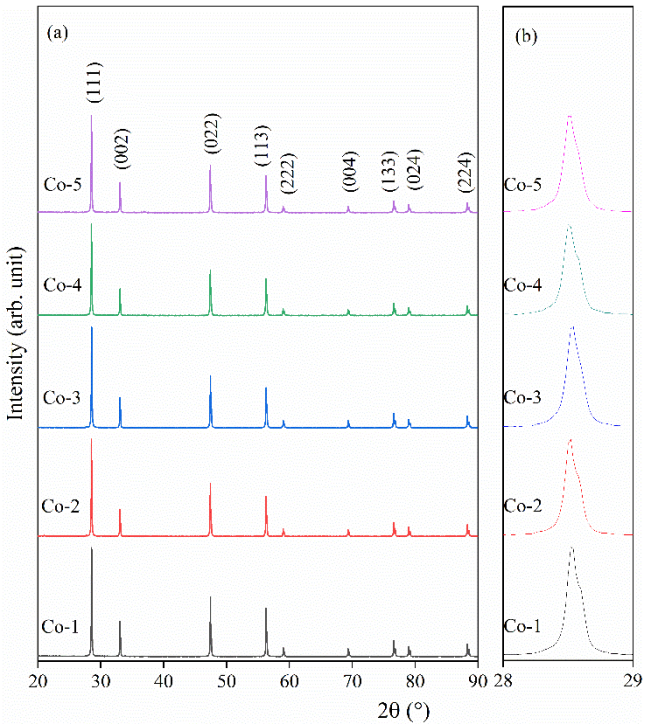

Fig. 4.4: (a) XRD pattern of Co-doped GDC powders (1-5 wt %) sintered at 1000°C (b) enlarged view of the (111) peak.

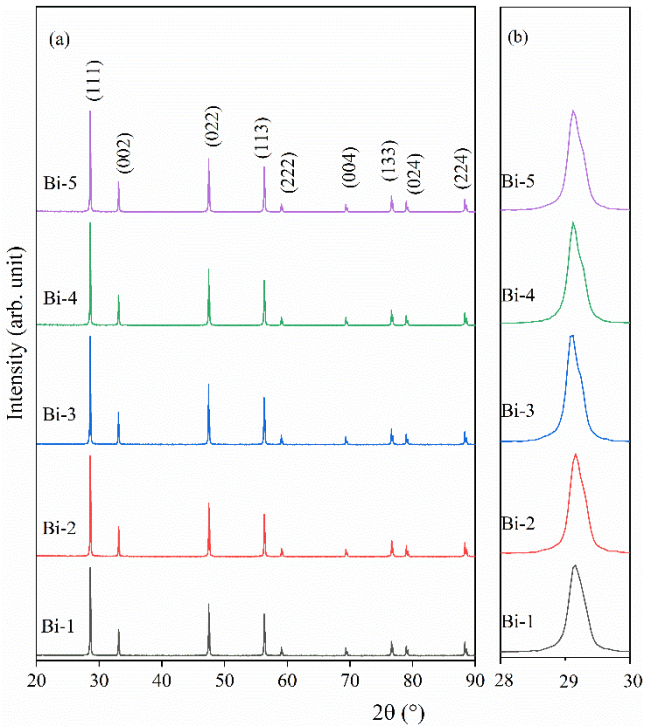

Fig. 4.5: (a) XRD pattern of Bi-doped GDC powders (1-5 wt %) sintered at 1200°C (b) enlarged view of the (111) peak.

XRD analysis has been carried out for the identification of the crystalline phase. The XRD patterns of the sintered samples of pure GDC, Cu- doped GDC, Co- doped GDC and Bi- doped GDC are shown in Fig. 4.2, 4.3(a), 4.4(a), 4.5(a) respectively. XRD analysis is successfully employed to characterize the crystal structure and phase composition of (Cu, Co, Bi) -doped GDC samples with varying weight ratios. There are multiple peaks and all the observed diffraction peaks are indexed with the standard ICDD-01-075-0161 card of Gadolinium Doped Ceria $Ce_{0.9}Gd_{0.1}O_{1.95}$ (space group number 225). A cubic fluorite structure with the space group Fm-3m is present in all of the samples. The XRD patterns show no secondary phases, which suggests that a single phase is formed in each sample. The addition of the sintering aid has little effect on the full width half maximum (fwhm) of sintered samples. For all of the sintered samples, the level of crystallinity is same. In accordance to the sintering aid concentration, as shown in Fig. 4.3(b), 4.4(b), 4.5(b) the XRD peaks shift towards the direction of the lower diffraction angle. The tensile strain caused by the dopants in the lattice leads to the shifting to the lower angle side.

The lattice parameter 'a' is calculated with the help of the given equations,

$$n\lambda = 2d\sin\theta \qquad \text{Equation 4-1}$$

$$d = \frac{a}{\sqrt{h^2 + k^2 + l^2}} \qquad \text{Equation 4-2}$$

where, d is the interplanar spacing, (hkl) are the miller indices of the crystalline planes.

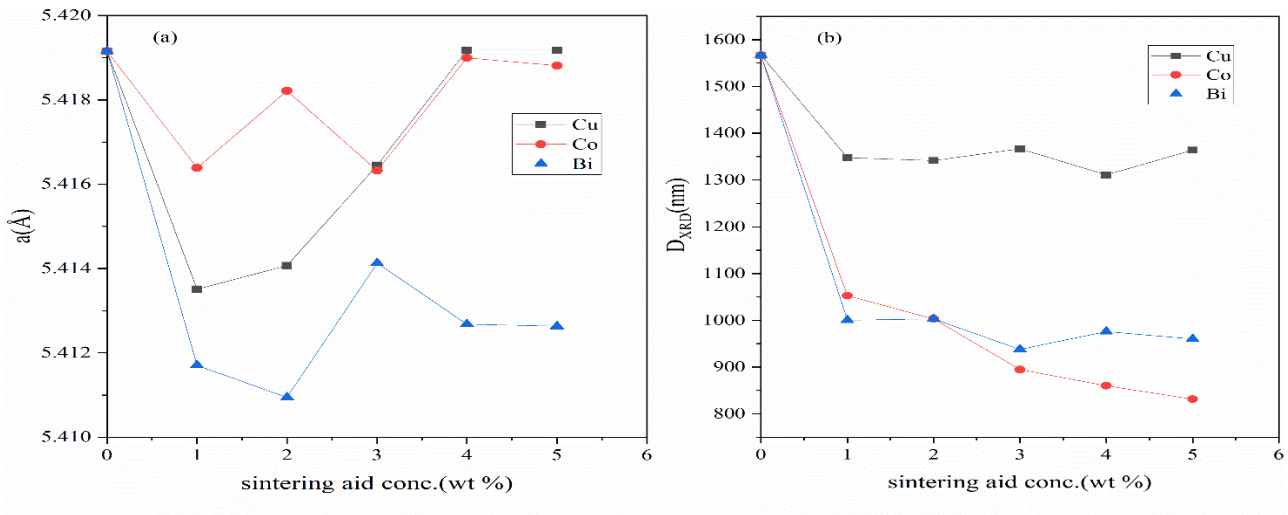

Fig. 4.6: (a) lattice parameter "a" of the samples w.r.t sintering aid concentration and (b) the crystallite size of the samples w.r.t sintering aid concentration.

Fig. 4.6(a) represents the lattice parameter “a” of the samples as a function of sintering aid concentration and from this it is observed that for Copper (Cu) and Cobalt (Co) the lattice parameter first decreases and then increases again with increase in sintering aid concentration. In Bismuth (Bi), it is seen that as the sintering aid concentration increases, the lattice parameter first decreases and then increases but did not reach the initial lattice parameter value that was the case with Cu and Co. This occurs due to the simultaneous effect of sintering aid concentration and sintering temperature. As the sintering temperature is lowered (1000 °C/ 1200 °C) than the initial sintering temperature (1450°C) with no sintering aid, the grains were not able to develop properly but with increasing sintering aid concentration density increases and thus lattice parameter is again shifting back to its initial original value. Fig. 4.6 (b) represents the crystallite size of the samples formed as a function of sintering aid concentration and it is observed that the crystallite size decreases with increase in sintering aid concentration.

4.3 SEM Analysis

Microstructures of the samples with varying ratios of sintering aids sintered at different temperatures are studied using SEM. Fig. 4.7 (a), (c) and 4.7 (b), (d) shows the SEM images of GDC samples sintered at 1450 °C and 1000 °C respectively. It is clearly observed that the fractured surface image (Fig. 4.7 (d)) of the GDC sample sintered at 1450 °C has higher density than that sintered at 1000 °C (Fig. 4.8(c)) and there is a 10-fold increase in the grain size of the GDC sample on from sintering temperature 1000 °C to 1450 °C as observed from Fig. 4.7(a),(b).

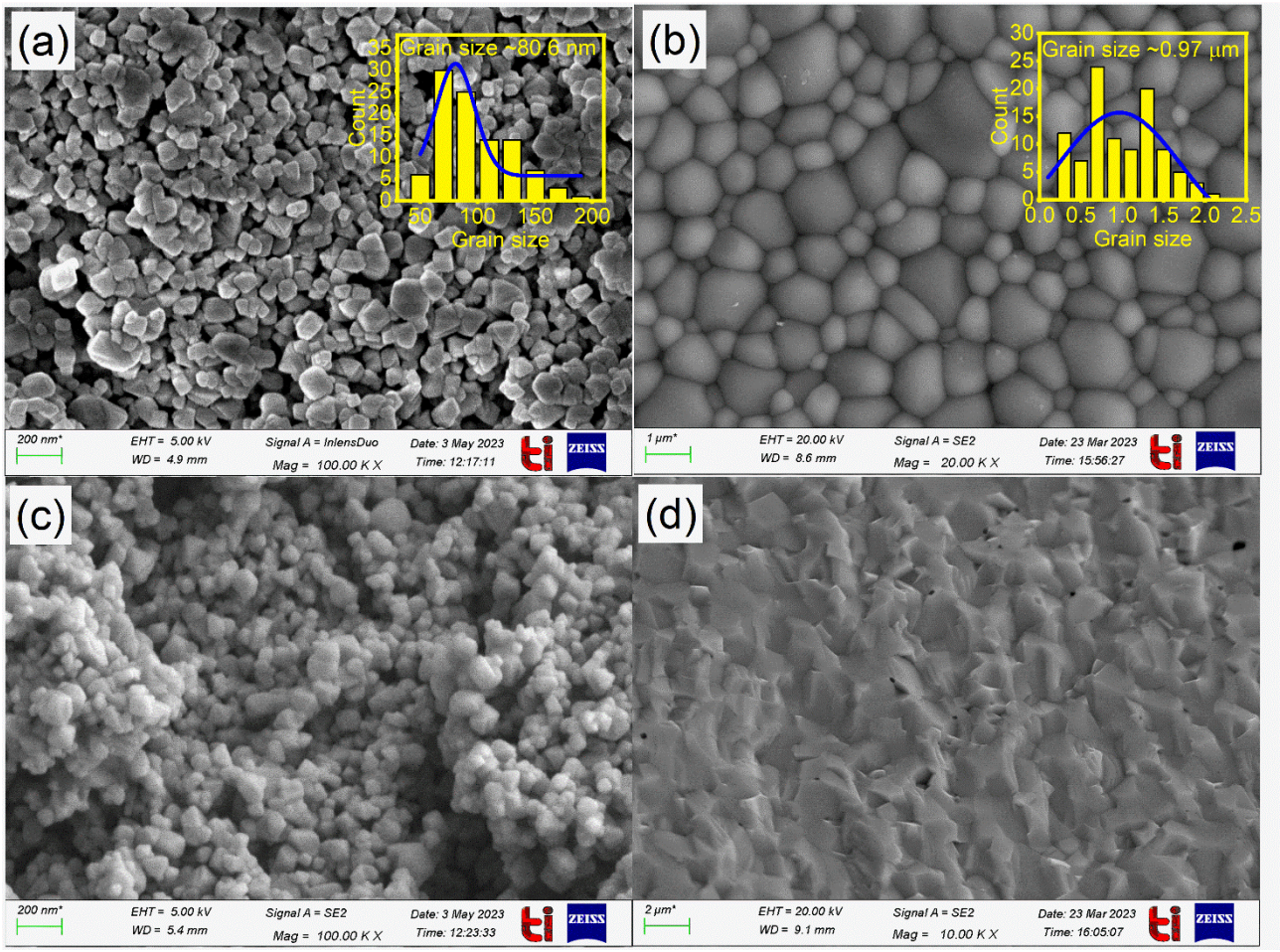

Fig. 4.7: SEM images of surface of GDC samples (a) sintered at 1000 °C for 4 h at magnification 100 Kx (b) sintered at 1450 °C for 4 h at magnification 20 Kx and of fractured surface (c) sintered at 1000 °C for 4 h at magnification 100 Kx (d) sintered at 1450 °C for 4 h at magnification 10 Kx.

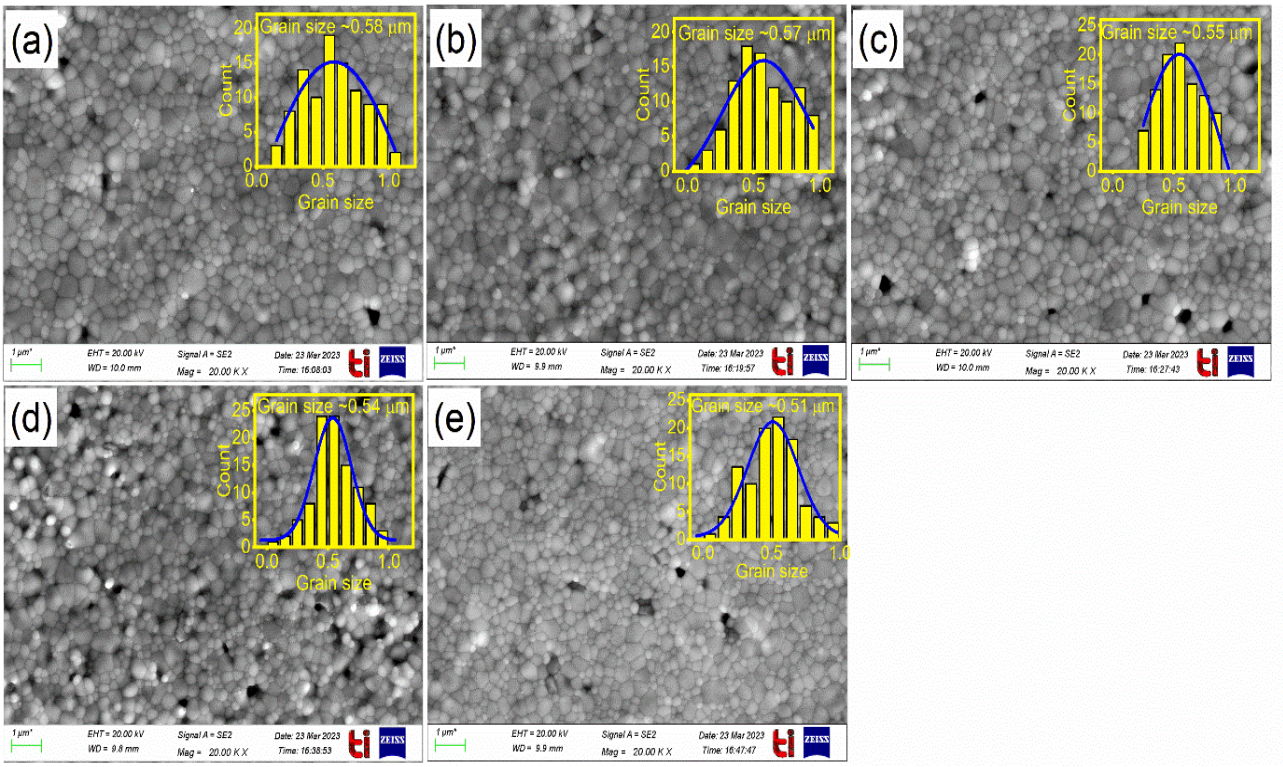

Fig. 4.8: SEM images of surface of Cu- doped GDC samples sintered at 1000 °C for 4 h at magnification 20 Kx (a) Cu-1 wt% (b) Cu-2 wt% (c) Cu-3 wt% (d) Cu-4 wt% (e) Cu-5 wt%.

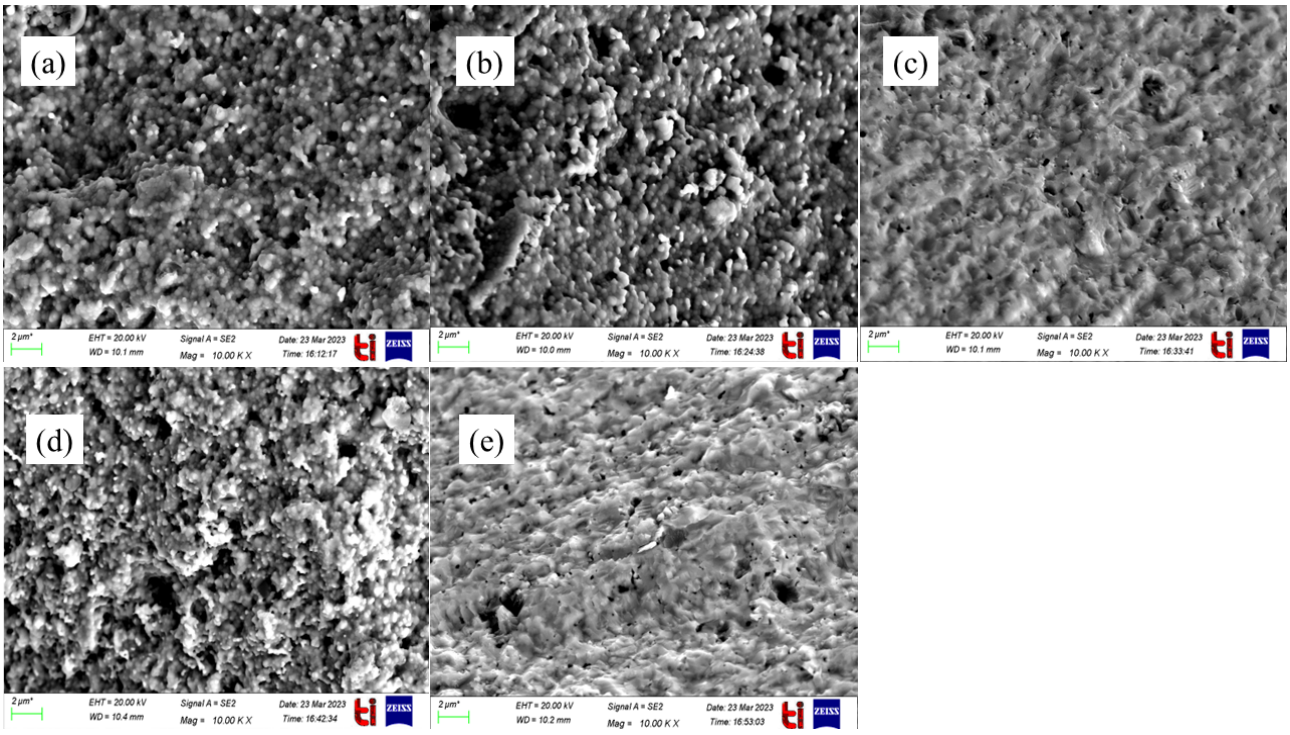

Fig. 4.9: SEM images of fractured surfaces of Cu- doped GDC samples sintered at 1000 °C for 4 h at magnification 10 Kx (a) Cu-1 wt% (b) Cu-2 wt% (c) Cu-3 wt% (d) Cu-4 wt% (e) Cu-5 wt%.

Fig. 4.8, 4.10 and 4.12 represents the surface SEM images of Cu- doped GDC, Co- doped GDC, Bi- doped GDC in varying ratios (1-5 wt %) respectively. From these SEM images it is seen that the grain size has decreased considerably with respect to initial GDC sample without sintering aid addition. Also, porosity decreases with increase in sintering temperature [43]. Fig. 4.9, 4.11, 4.13 represents about the fractured surface pictures of the Cu- doped GDC (1-5 wt %), Co- doped GDC (1-5 wt %), Bi- doped GDC (1-5 wt %) respectively. The density is found to be increasing with increase in sintering aid concentration as observed from the SEM images of the fractured surfaces.

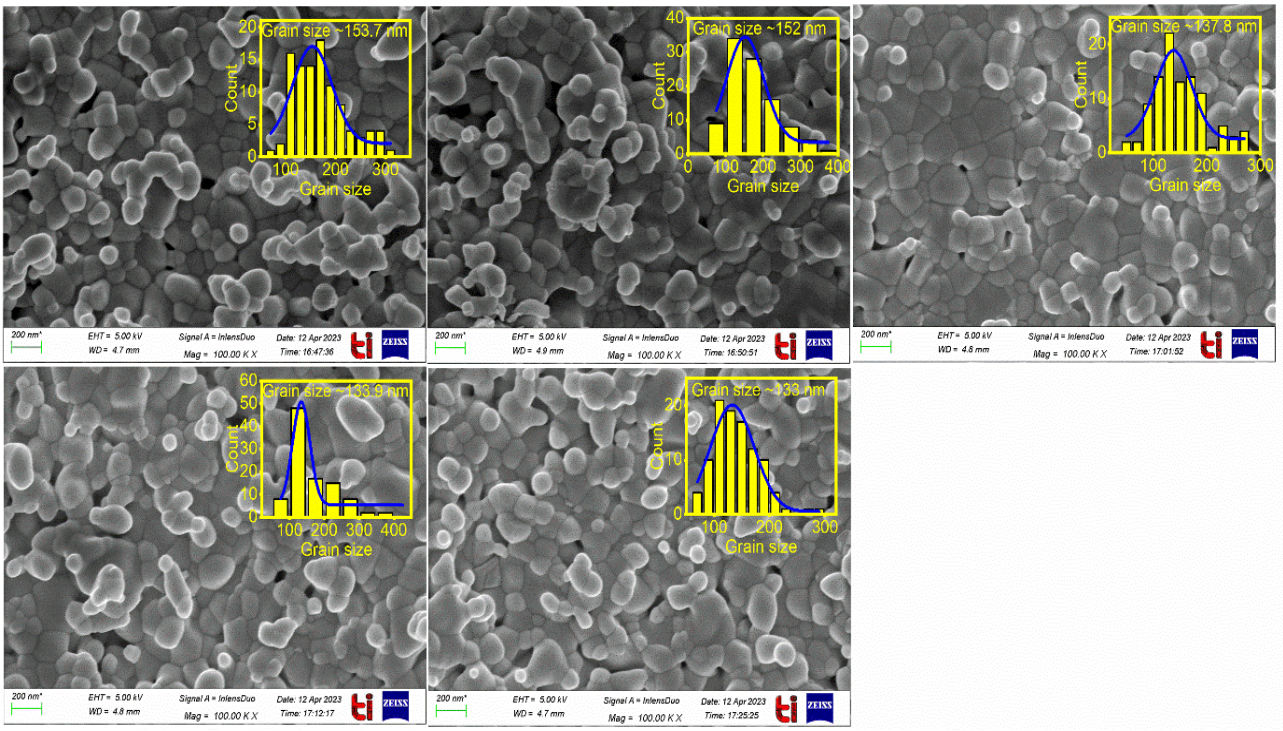

Fig. 4.10: Surface morphology of Co- doped GDC samples sintered at 1000 °C for 4 h at magnification 100 Kx (a) Co-1 wt% (b) Co-2 wt% (c) Co-3 wt% (d) Co-4 wt% (e) Co-5 wt%.

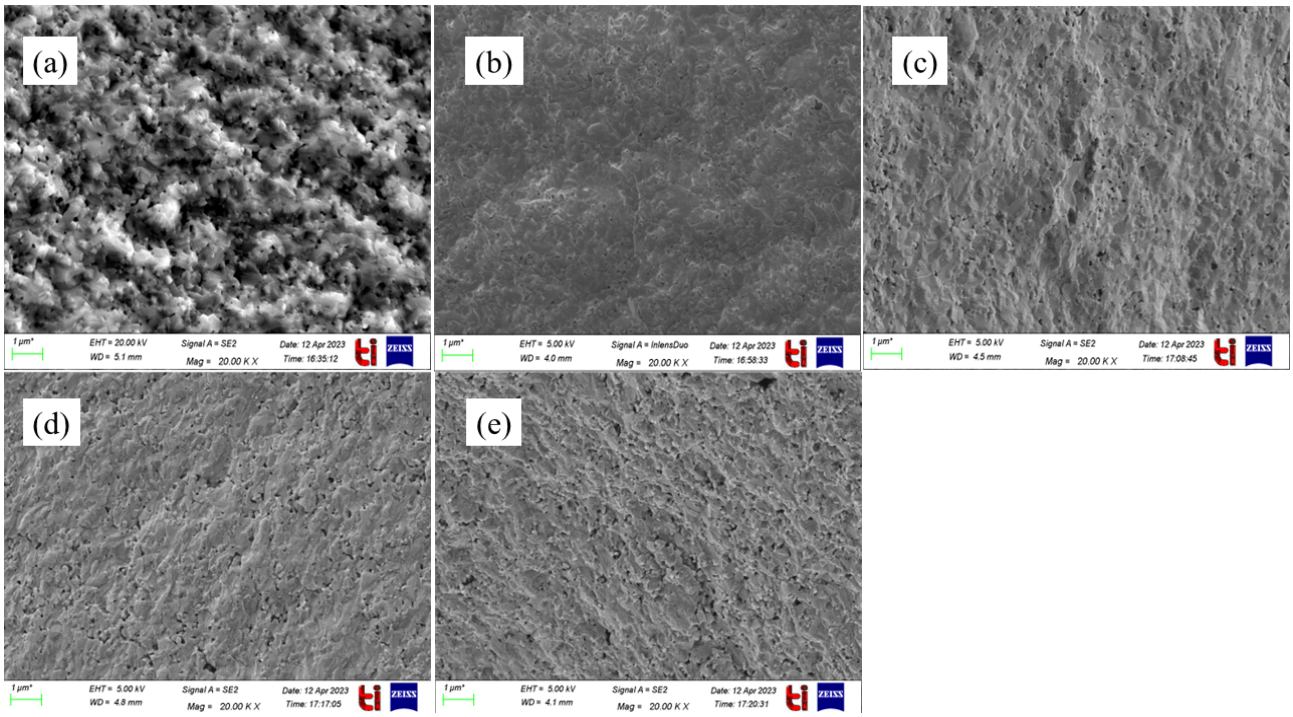

Fig. 4.11: SEM images of fractured surface of Co- doped GDC samples sintered at 1000 °C for 4 h at magnification 20 Kx (a) Co-1 wt% (b) Co-2 wt% (c) Co-3 wt% (d) Co-4 wt% (e) Co-5 wt%.

For 1 wt% and 2 wt% of each Co, Cu and Bi as sintering aids, the SEM images show less density, but in 3 wt% images of all the samples the density drastically increases. All the grains are seen connected to each other and this shows that liquid phase sintering mechanism occurs. Also, from SEM images it is clearly seen that melting of sintering aids takes place causing liquid phase sintering which is the reason for higher densities. But much higher sintering aid concentration leads to porosity [44], as seen in Fig. 4.9 (e), 4.11 (e) and 4.13 (e). This is may be the result of more liquid-phase sintering due to greater sintering aid concentration. Along with smaller grains and more grain boundaries, this porosity contributes to the reduction in the density of the samples with sintering aid concentration greater than 3 wt %.

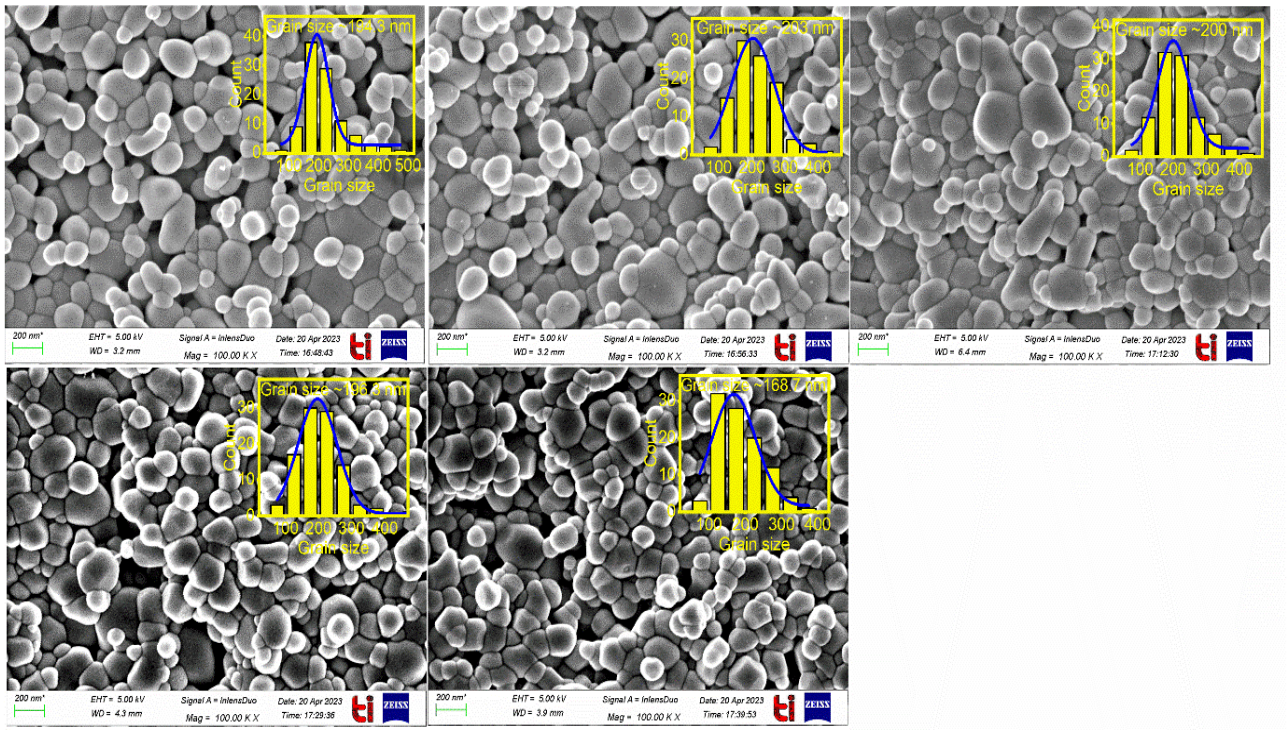

Fig. 4.12: SEM images of surface of Bi- doped GDC samples sintered at 1200 °C for 4 h at magnification 100 Kx (a) Bi-1 wt% (b) Bi-2 wt% (c) Bi-3 wt% (d) Bi-4 wt% (e) Bi-5 wt%.

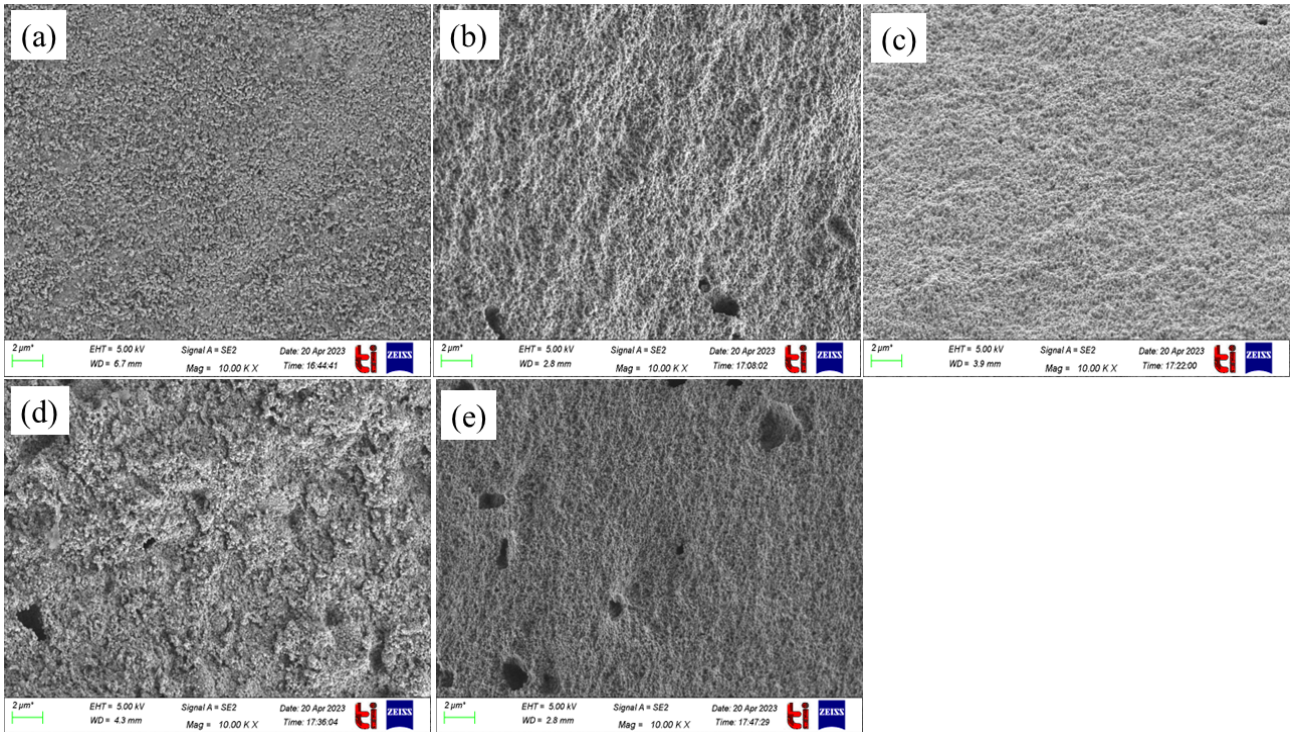

Fig. 4.13: SEM images of fractured surface of Bi- doped GDC samples sintered at 1200 °C for 4 h at magnification 10 Kx (a) Bi-1 wt% (b) Bi-2 wt% (c) Bi-3 wt% (d) Bi-4 wt% (e) Bi-5 wt%.

From SEM images Fig. 4.8, 4.10 and 4.12 it is clearly observed that with increase in sintering aid concentration, the overall average grain size reduces and it is very less than the average grain size of the initial pure GDC sample. GDC sintered at 1450 °C has grain size 0.97 µm whereas sintered at 1000°C has grain size 80.6 nm. The addition of sintering aid inhibits the grain growth leading to smaller grains in Cu, Co and Bi doped GDC samples than pure GDC samples. The grain size follows the order Co< Bi< Cu. This shows that Co inhibits the grain growth to the maximum extent and the particles are almost nano-sized whereas Cu has highest grain size amongst all which indicates that Cu does not have much effect on grain size. The average grain size for all the sintered samples is shown below (Fig. 4.14):

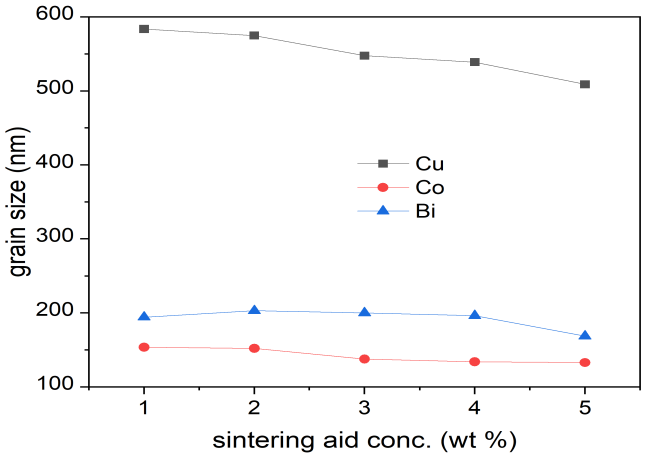

Fig. 4.14: Average grain size of the samples (Cu, Co, Bi) w.r.t sintering aid concentration.

4.4 Conductivity Analysis

The ionic conductivity of formed pellets has been measured using a symmetric cell design by AC impedance spectroscopy. Fig. 4.15 (a), (b), (c) represents the Cole- Cole plots for GDC, Cu- doped GDC (3 wt%), Co- doped GDC (3 wt%) and Bi- doped GDC (3 wt%). GDC possesses very high density and an excellent microstructure when sintered at 1450 ºC. Thus, in order to conduct a conductivity analysis, this sample was chosen. Two semicircles have been observed for GDC sample when measured at 600 ºC. Similar is the case seen in Cu- 3 wt% and Co- 3 wt% samples. But Bi- 3 wt% exhibit three semicircles. The first semicircle shows the contribution of grains, the second tells about the contribution of the grain boundaries and the third semicircle is linked to electrode contribution. Only the grain boundary arc is visible for GDC, Cu and Co. Whereas both the grain and grain boundary arcs are seen in the case of Bi followed by the electrolyte/electrode contact. This visibility of three semicircles at high temperatures and of two semicircles at low temperature depends on the nature of samples and

also on the experimental conditions [45], [20]. The first and second semicircle is fitted by connecting two circuits in series in which R_{grain} and CPE_{grain} connected in parallel whereas the third semi-circle's fitting is identical to the circuit used for the second semi-circle, but with an additional $CPE_{electrode}$ connected in series to it. The total conductivity is the sum of the grain and the grain boundary conductivity. The grain and the grain boundary arc vanish as the temperature rises. When the sample is sintered at high temperatures, cations of sintering aid may segregate along the grain boundaries, which may account for this phenomenon. Due to thermal energy, they move more quickly at high temperatures. The grain boundary resistance is raised by the segregation of these contaminants along the grain boundaries [46]. A single semicircle results when the electrode resistance that contributes the most to overall resistance i.e., the grain and grain boundary resistance becomes independent of frequency [20].

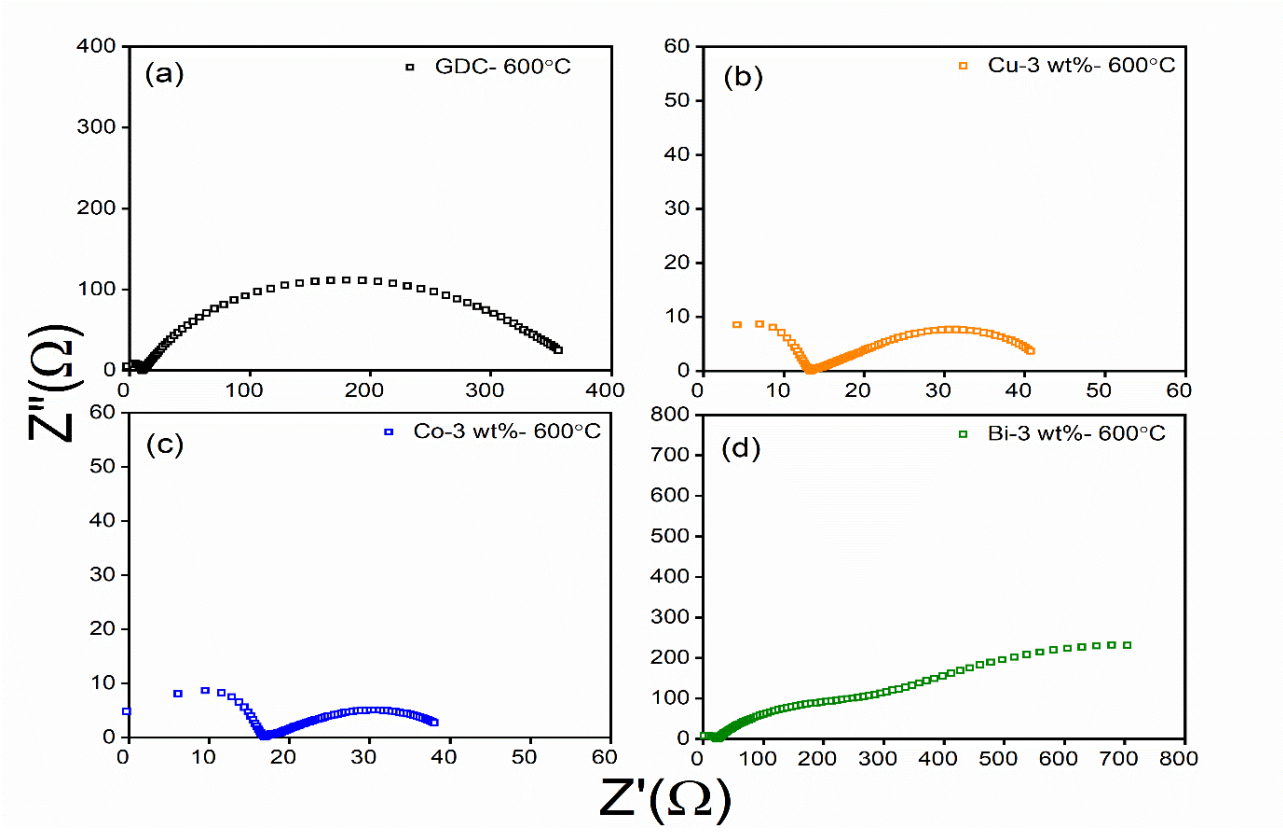

Fig. 4.15: Cole-Cole plot of (a) GDC pellet sintered at 1450 ºC (b) Cu- 3 wt% pellet sintered at 1000 ºC (c) Co- 3 wt% pellet sintered at 1000 ºC (d) Bi- 3 wt% pellet sintered at 1200 ºC in the temperature 600 ºC.

Fig. 4.16 represents the conductivity of sintered samples with sintering aid concentration in various ratios. It is observed from this graph that the conductivity of the samples first increases with increase in sintering aid concentration and then decreases with increasing sintering aid

concentration. Pure GDC sample has the conductivity 1.031 x 10^{-2} S cm^{-1}. And for Cu, Co and Bi conductivity results comes out to be 1.182 x 10^{-2} S cm^{-1}, 1.237x 10^{-2} S cm^{-1}, 0.81 x10^{-2} S cm^{-1} respectively. In this study, the additions of sintering aids raise the conductivity of Gadolinium Doped Ceria in the order Cu< Co except Bi. Using the Arrhenius equation, the effective Activation energy (E_a) for conduction has been measured:

$$\sigma_T = \sigma_0 \exp\left(\frac{-E_a}{kT}\right) \qquad \text{Equation 4-3}$$

where, σ_T is the total conductivity, σ_0 is the pre-exponential factor, k is the Boltzmann's constant, E_a is the activation energy.

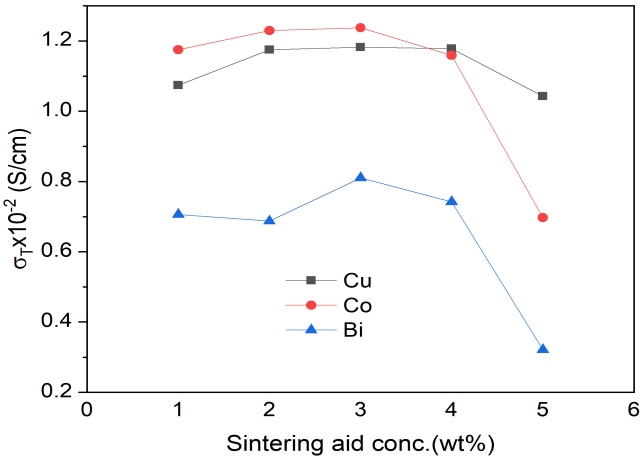

Fig. 4.16: Conductivity of of the samples (Cu, Co, Bi) w.r.t sintering aid concentration.

The variation of $\ln\sigma_T$ as a function of temperature is depicted in Fig. 4.17. The activation energy (E_a) of GDC sintered at 1450 ºC is 1.294 eV and possesses a single slope. With the addition of sintering aids and decreasing temperature, the graphs showed two slopes corresponding to two activation energies. One single straight line cannot fit the Arrhenius plots of ceria electrolyte with sintering aids. As a result, it can be assumed that at a certain transition temperature, the conduction mechanism alters [47]. In the Arrhenius curve, there are two regions where the slope varies, one associated with the low-temperature and the other with the high-temperature. Consequently, the activation energy varies with temperature [20]. The high temperature regime has less activation energy as less energy is required to cross the barrier whereas low temperature domain should possess high activation energies. All the samples follow the same behavior having less values of activation energy in the high temperature domain and high activation energy values in the low temperature regime.

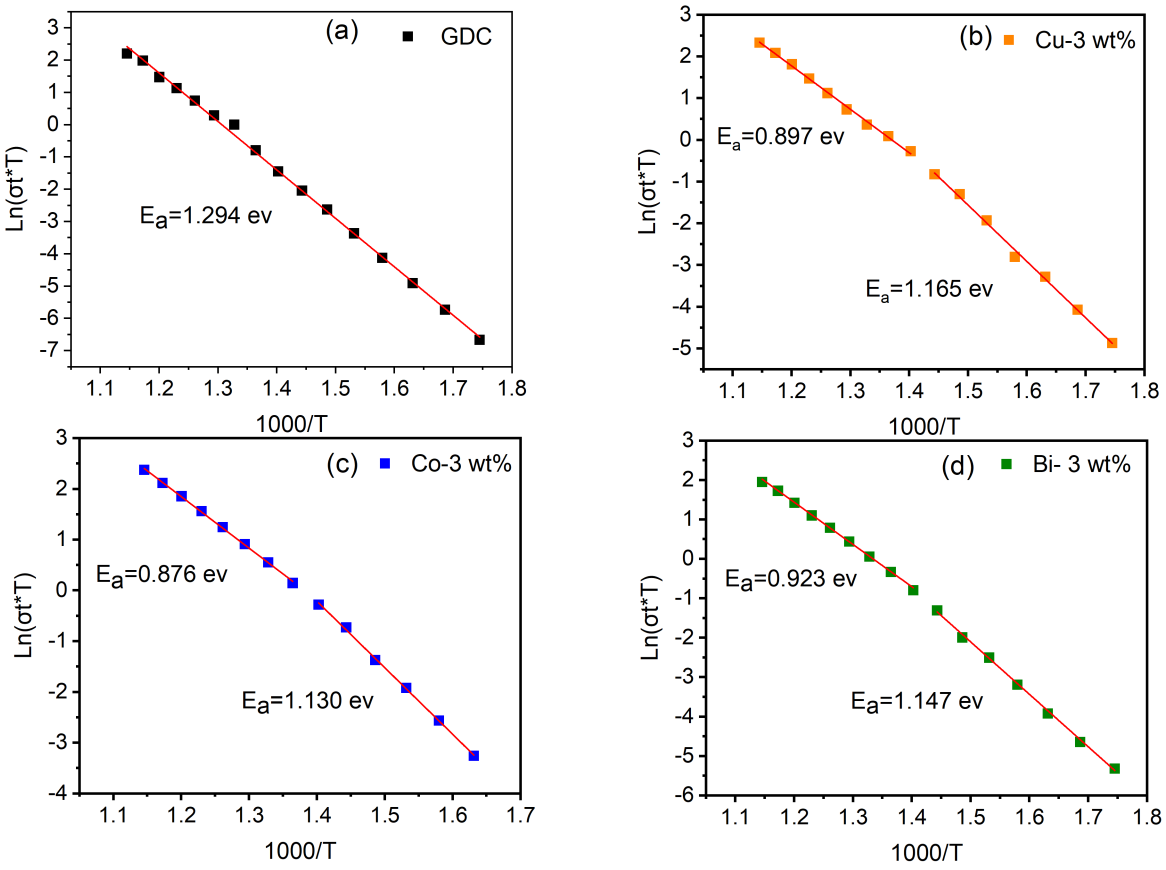

Fig. 4.17: Arrhenius plots of total conductivity of (a) GDC sintered at 1450 ºC (b) Cu- 3 wt % sintered at 1000 ºC (c) Co- 3 wt% sintered at 1000 ºC (d) Bi- 3 wt % sintered at 1200 ºC.

4.5 Cell fabrication and characterization

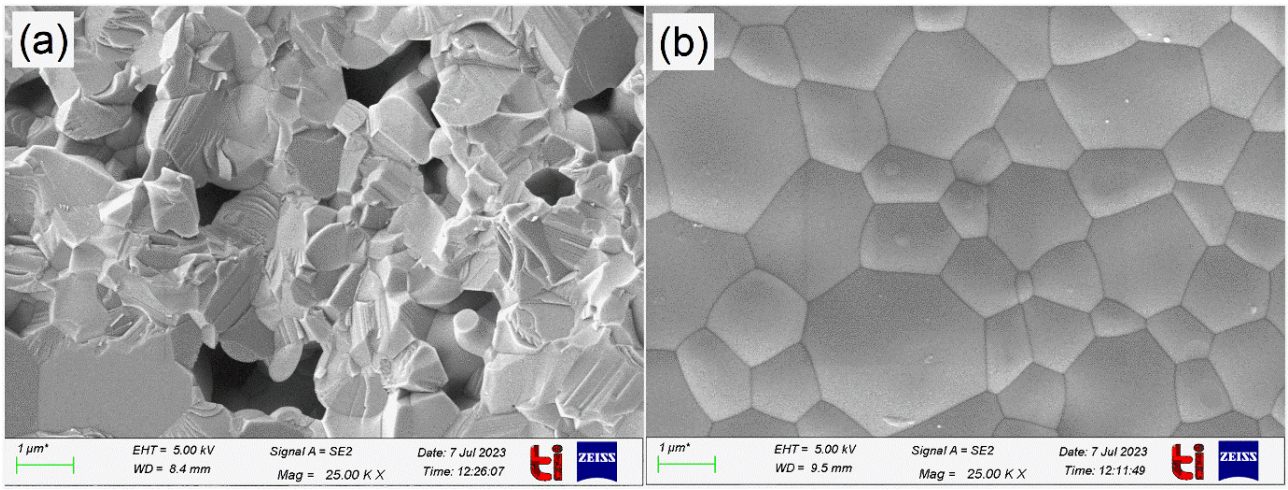

Fig. 4.18: SEM images of (a) Anode surface (b) Electrolyte surface of GDC sintered at 1450ºC at 25 Kx magnification.

Fig. 4.18 represents the anode and electrolyte surface of pure GDC sample sintered at 1450ºC. From its SEM images, it has been clearly observed that the anode surface is highly porous and its electrolyte surface possesses is very dense. GDC has an average grain size of 1.26 µm and has very high conductivity of 1.031 x 10^{-2} S cm^{-1}. Hence, GDC samples sintered at 1450ºC is considered as best suitable for SOFCs and thus considered as a best suited reference to discover more efficient materials for use in SOFC.

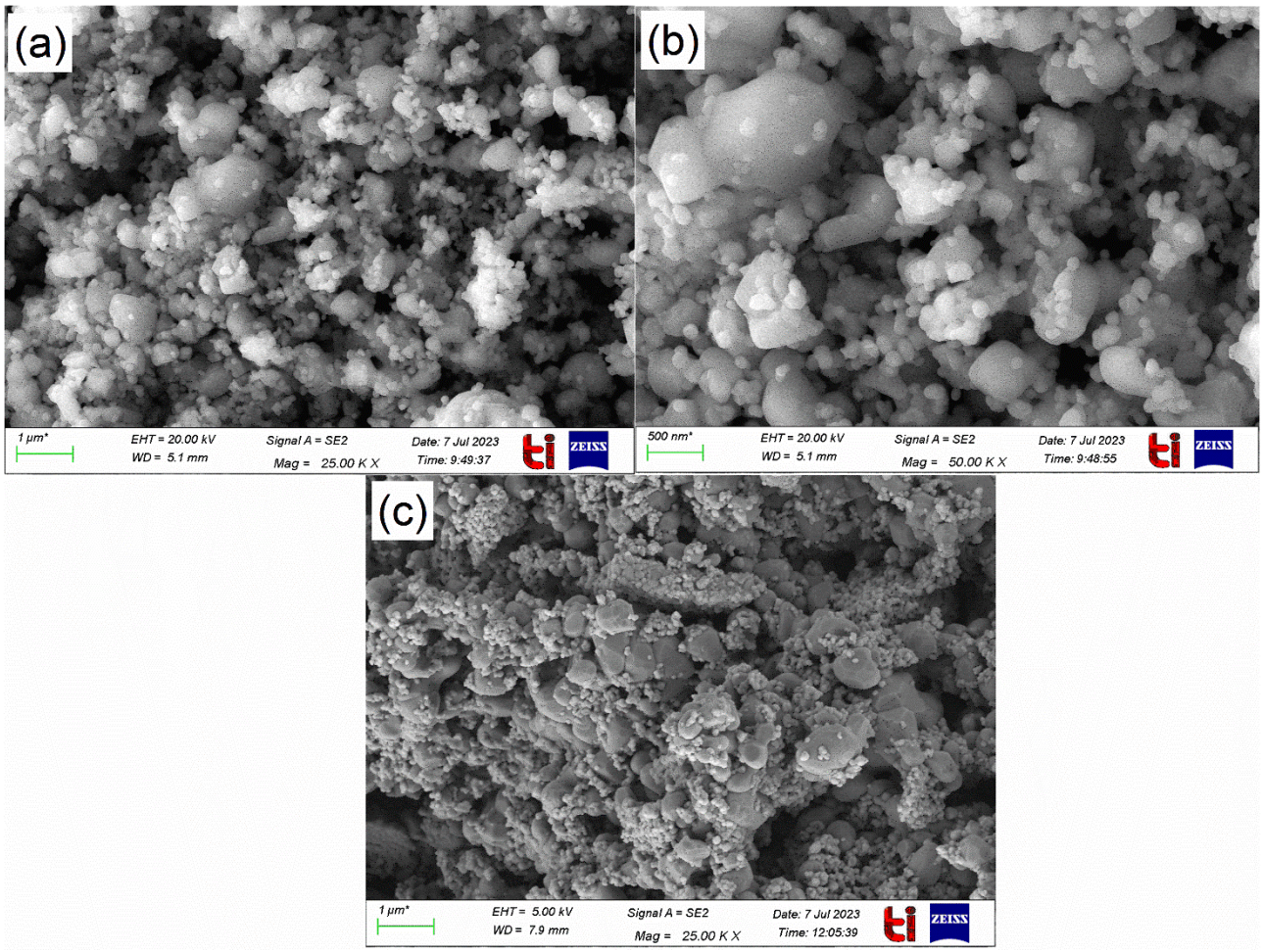

Fig. 4.19: SEM images of Anode surface of (a) Cu- 3wt% (b) Co- 3 wt% (c) Bi- 3 wt% doped GDC samples sintered at 1000 ºC.

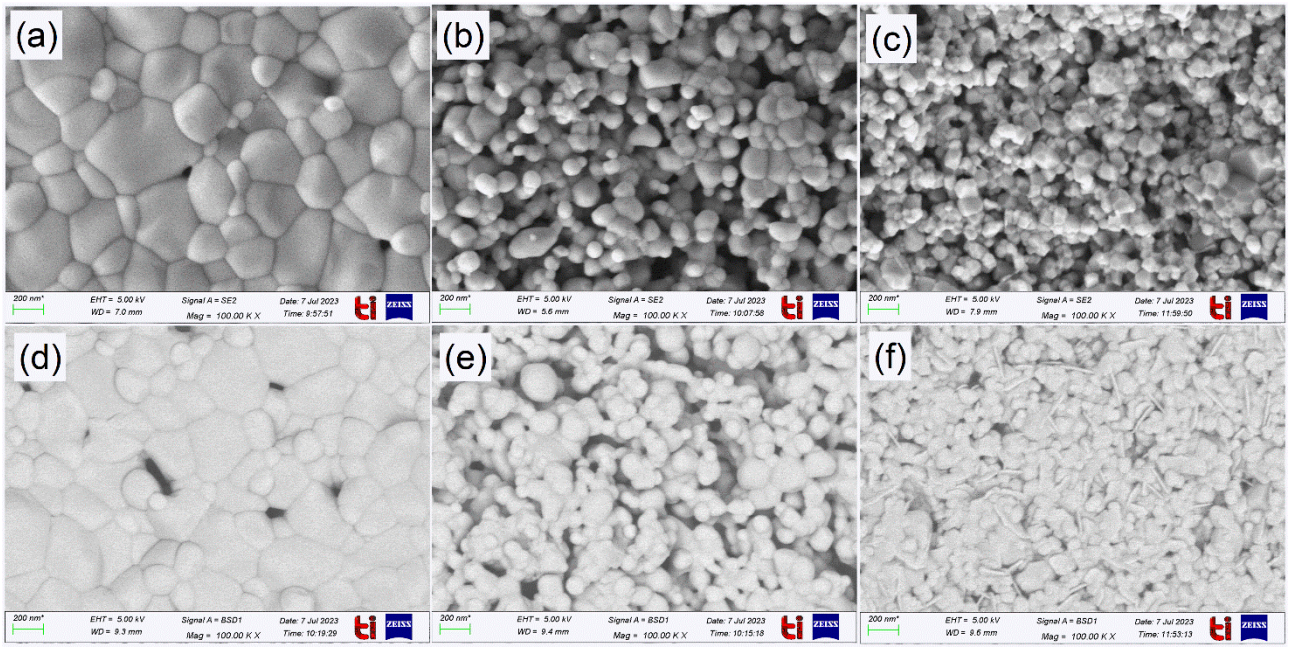

Fig. 4.20: SEM images of electrolyte surface and backscattered electrolyte surface of (a) Cu- 3wt% (b) Co- 3 wt% (c) Bi- 3 wt% doped GDC samples sintered at 1000 ºC at 100 Kx magnification.

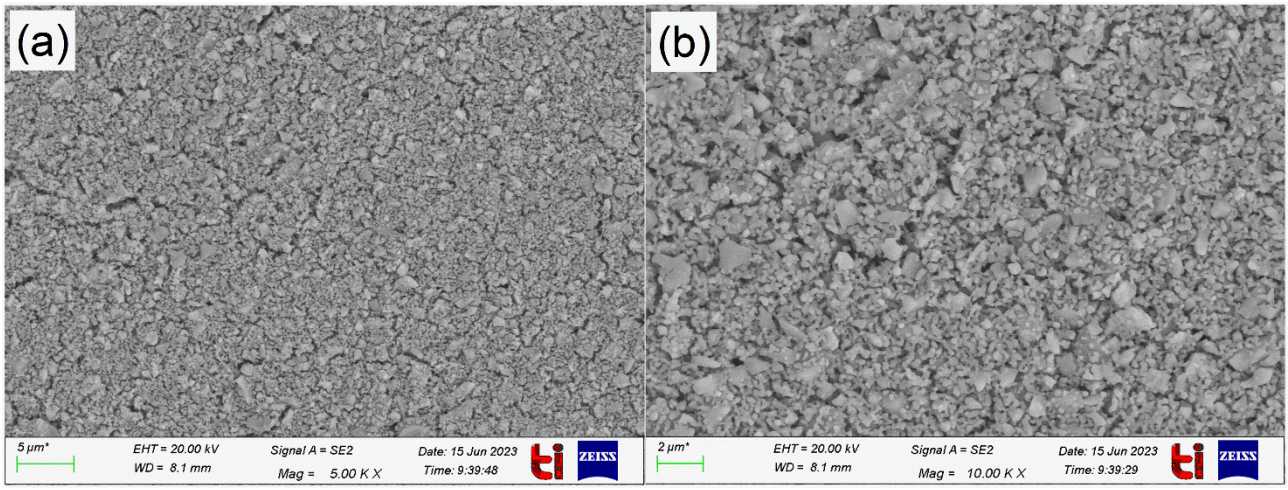

Fig. 4.21: SEM image of surface of (a) cathode LSCF: GDC surface at 10 Kx magnification (b) cathode LSCF: GDC surface sintered at 1000 ºC at 5 Kx magnification.

Fig. 4.19 (a), (b) and (c) represents the anode surface of GDC samples with Cu- 3 wt%, Co- 3 wt% and Bi- 3 wt% sintering aid respectively. It has been observed from the anode surface images that the anode surface is porous. Fig. 4.20 (a), (b) and (c) represents the electrolyte surface of GDC samples with Cu- 3 wt%, Co- 3 wt% and Bi- 3 wt% sintering aid respectively and Fig. 4.20 (d), (e) and (f) represents the backscattered electrolyte surface images of GDC samples with Cu- 3 wt%, Co- 3 wt% and Bi- 3 wt% sintering aid respectively. The average

grain size of GDC samples with Cu- 3 wt%, Co- 3 wt% and Bi- 3 wt% is 263.2 nm, 107.5 nm and 76.9 nm, respectively. Backscattered images represents that no secondary phase is formed and the electrolyte surface images shows that the surface is dense. Also, it has been clearly seen that the Cu is having most dense surface. Fig. 4.21 (a) and (b) shows the cathode surface images of LSCF-GDC composite and from cathode images it has been observed that the surface is uniform but contains pin holes. This may be due to the brush painting of cathode ink.

SUMMARY

The effects of Cu, Co and Bi as a sintering aid in Gadolinium Doped Ceria ($Gd_{0.1}Ce_{0.9}O_{1.95}$) has been studied. All the prepared GDC powders with different sintering aid ratios are characterized with XRD, SEM and impedance analysis. The sintered samples possess single phase Cubic Fluorite structure. No additional phase was formed and the results reflect that the oxides of sintering aids increase the sinterability of $Gd_{0.1}Ce_{0.9}O_{1.95}$ to various extents, lowering its sintering temperature by 300-400 ºC. The sintering aid concentration has a minimal effect on the lattice parameters of Gadolinium Doped Ceria. Sintering aid additions favours Liquid Phase Sintering. Also, Cu and Co samples enhances the conductivity of GDC material whereas Bi additions has less conductivity than pure GDC sample. The conductivity increases in the order Bi< Cu< Co. 3 wt% additions of all the sintering aids shows the best results upon characterizing. They have minimum effect on the electrical properties and possess higher densities (97.3%, 95.5% and 94.5%) and increased conductivity (1.182×10^{-2} S cm^{-1}, 1.237×10^{-2} S cm^{-1}, 0.81×10^{-2} S cm^{-1}) for Cu, Co and Bi respectively than other ratios (1, 2, 4, 5 wt%).

FUTURE SCOPE

- The primary drawback of utilizing sintering aids to reduce the sintering temperature of GDC is that they persist at the boundaries of the grains upon sintering and may have a negative impact by causing electrical conduction or lowering the oxygen ion conductivity that should be reduced.
- Optimization of better properties for anode and cathode samples can be done to increase the performance of IT-SOFCs.
- Cell testing can be done with the prepared samples having sintering aids for achieving improved power density results.
- More research can be done on employing Cu as a sintering aid has it has good results.
- More optimized sintering aids must be employed in suitable varying ratios to increase the power density of the SOFC system.

REFERENCES

1. Pike, T.W., *Development and processing of solid oxide fuel cell materials.* 2015.
2. Ryan, P., *O'Hayre Author, Fuel Cell Fundamentals/Ryan O'Hayre, Suk-Won Cha, Whitney G. Colella, Fritz B. Prinz.* 2016.
3. Choi, H.-J., et al., *Development of solid oxide cells by co-sintering of GDC diffusion barriers with LSCF air electrode.* Ceramics International, 2017. **43**(16): p. 13653-13660.
4. Minh, N.Q., *Solid oxide fuel cell technology—features and applications.* Solid State Ionics, 2004. **174**(1-4): p. 271-277.
5. Singhal, S.C., *Solid oxide fuel cells for stationary, mobile, and military applications.* Solid State Ionics, 2002. **152**: p. 405-410.
6. Badwal, S.P.S. and K. Foger, *Solid oxide electrolyte fuel cell review.* Ceramics International, 1996. **22**(3): p. 257-265.
7. Zarkov, A., et al., *Synthesis of nanocrystalline gadolinium doped ceria via sol–gel combustion and sol–gel synthesis routes.* Ceramics International, 2016. **42**(3): p. 3972-3988.
8. Song, X., *Effect of additives on sintering and conductivity of yttria-stabilized zirconia.* 2016.
9. Haile, S.M., *Fuel cell materials and components.* Acta materialia, 2003. **51**(19): p. 5981-6000.
10. Fergus, J.W., *Electrolytes for solid oxide fuel cells.* Journal of power sources, 2006. **162**(1): p. 30-40.
11. Strickler, D.W. and W.G. Carlson, *Ionic conductivity of cubic solid solutions in the system cao—y2o3—zro2.* Journal of the American Ceramic Society, 1964. **47**(3): p. 122-127.
12. Verkerk, M.J., A.J.A. Winnubst, and A.J. Burggraaf, *Effect of impurities on sintering and conductivity of yttria-stabilized zirconia.* Journal of Materials Science, 1982. **17**: p. 3113-3122.
13. Sammes, N.M., et al., *Bismuth based oxide electrolytes—structure and ionic conductivity.* Journal of the European Ceramic Society, 1999. **19**(10): p. 1801-1826.
14. Tianshu, Z., et al., *Ionic conductivity in the CeO2–Gd2O3 system (0.05≤ Gd/Ce≤ 0.4) prepared by oxalate coprecipitation.* Solid State Ionics, 2002. **148**(3-4): p. 567-573.

15. Santos, T.H., et al., *Structure, densification and electrical properties of Gd3+ and Cu2+ co-doped ceria solid electrolytes for SOFC applications: Effects of Gd2O3 content.* Ceramics International, 2018. **44**(3): p. 2745-2751.
16. German, R.M., P. Suri, and S.J. Park, *Liquid phase sintering.* Journal of materials science, 2009. **44**: p. 1-39.
17. Reuterdahl, O., *Production of Fe-TiB2composite using liquidphase sintering*. 2013.
18. Sigl, L.S. and K.A. Schwetz, *TiB sub 2-based cemented borides: A new generation of hardmetals.* Powder Metallurgy International;(Germany), 1991. **23**(4).
19. Pikalova, E.Y., et al., *Effect of doping with Co 2 O 3, TiO 2, Fe 2 O 3, and Mn 2 O 3 on the properties of Ce 0.8 Gd 0.2 O 2− δ.* Inorganic Materials, 2007. **43**: p. 735-742.
20. Accardo, G., C. Ferone, and R. Cioffi, *Influence of Lithium on the Sintering Behavior and Electrical Properties of $Ce_{0.8}Gd_{0.2}O_{1.9}$ for Intermediate-Temperature Solid Oxide Fuel Cells.* Energy Technology, 2016. **4**(3): p. 409-416.
21. German, R.M., P. Suri, and S.J. Park, *Review: liquid phase sintering.* J. Mater. Sci, 2009. **44**(1): p. 1-39.
22. Nicholas, J.D. and L.C. De Jonghe, *Prediction and evaluation of sintering aids for cerium gadolinium oxide.* Solid State Ionics, 2007. **178**(19-20): p. 1187-1194.
23. Roy, J., *The effect of strontium doping on densification and electrical properties of Ce0. 8Gd0. 2O2− δ electrolyte for IT-SOFC application.* Ionics, 2012. **18**(3): p. 291-297.
24. Taub, S., et al., *The effects of Co and Cr on the electrical conductivity of cerium gadolinium oxide.* Solid State Ionics, 2015. **282**: p. 54-62.
25. Dasari, H.P., et al., *Record-low sintering-temperature (600° C) of solid-oxide fuel cell electrolyte.* Journal of Alloys and Compounds, 2016. **672**: p. 397-402.
26. Biesuz, M., et al., *Conventional and field-assisted sintering of nanosized Gd-doped ceria synthesized by co-precipitation.* Ceramics International, 2016. **42**(10): p. 11766-11771.
27. Valdebenito, J.U., A. Akbari-Fakhrabadi, and M.R. Viswanathan, *Effect of flash sintering on microstructure of $Ce_{0.9}Gd_{0.1}O_{1.95}$ electrolyte fabricated by tape-casting.* Materials Letters, 2017. **209**: p. 291-294.
28. Jamil, S.M., et al., *Anode supported micro-tubular SOFC fabricated with mixed particle size electrolyte via phase-inversion technique.* International Journal of Hydrogen Energy, 2017. **42**(14): p. 9188-9201.
29. Spiridigliozzi, L., et al., *Microstructural and electrical investigation of flash-sintered Gd/Sm-doped ceria.* Journal of materials science, 2017. **52**(12): p. 7479-7488.

30. Accardo, G., et al., *Improved microstructure and sintering temperature of bismuth nano-doped GDC powders synthesized by direct sol-gel combustion.* Ceramics International, 2018. **44**(4): p. 3800-3809.
31. Accardo, G., et al., *Morphology and Structural Stability of Bismuth-Gadolinium Co-Doped Ceria Electrolyte Nanopowders.* Inorganics, 2019. **7**(10): p. 118.
32. Mangifesta, P., A. Sanson, and E. Roncari, *Effect of the Doping Method on the Sintering Characteristics of Gadolinium-Doped Ceria.*
33. Biesuz, M. and V.M. Sglavo, *Flash sintering of ceramics.* Journal of the European Ceramic Society, 2019. **39**(2-3): p. 115-143.
34. Accardo, G., et al., *Optimized lithium-doped ceramic electrolytes and their use in fabrication of an electrolyte-supported solid oxide fuel cell.* International Journal of Hydrogen Energy, 2019. **44**(23): p. 12138-12150.
35. Accardo, G., et al., *Direct addition of lithium and cobalt precursors to $Ce_{0.8}Gd_{0.2}O_{1.95}$ electrolytes to improve microstructural and electrochemical properties in IT-SOFC at lower sintering temperature.* CERAMICS INTERNATIONAL, 2019. **45**(7): p. 9348-9358.
36. Grilo, J.P., et al., *Performance of GDC with alkali metal carbonates as sintering aids.* Solid State Ionics, 2020. **346**: p. 115221.
37. Wang, Z., et al., *Structures and electrical conductivities of Gd^{3+} and Fe^{3+} co-doped cerium oxide electrolytes sintered at low temperature for ILT-SOFCs.* Ceramics International, 2018. **44**(9): p. 10328-10334.
38. GÜÇTaŞ, D., V. SaribоĞA, and M.A.F. ÖKsÜZÖMer, *Microstructure and ionic conductivity investigation of samarium doped ceria (Sm0. 2Ce0. 8O1. 9) electrolytes prepared by the templating methods.* Turkish Journal of Chemistry, 2022. **46**(3): p. 910-922.
39. Cullity, B.D., *Elements of X-ray Diffraction*. 1956: Addison-Wesley Publishing.
40. Vinila, V.S. and J. Isac, *Synthesis and structural studies of superconducting perovskite GdBa2Ca3Cu4O10. 5+ δ nanosystems*, in *Design, Fabrication, and Characterization of Multifunctional Nanomaterials*. 2022, Elsevier. p. 319-341.
41. Seiler, H., *Secondary electron emission in the scanning electron microscope.* Journal of Applied Physics, 1983. **54**(11): p. R1-R18.
42. Il'ina, E.A., et al., *Sol-gel synthesis of Al-and Nb-co-doped Li 7 La 3 Zr 2 O 12 solid electrolytes.* Ionics, 2020. **26**: p. 3239-3247.

43. Kaur, T., et al., *Structural and Electrical Properties of Gd Doped CeO2 (GDC) Nanoceramics for Solid Oxide Fuel Cell Applications.* Transactions of the Indian Ceramic Society, 2022. **81**(3): p. 127-132.
44. Kaur, T., K. Singh, and J. Kolte, *Effect of intrinsic and extrinsic oxygen vacancies on the conductivity of Gd-doped CeO2 synthesized by a sonochemical route.* The Journal of Physical Chemistry C, 2022. **126**(42): p. 18018-18028.
45. Kazlauskas, S., et al., *Effect of sintering temperature on electrical properties of gadolinium-doped ceria ceramics.* Journal of materials science, 2015. **50**(8): p. 3246-3251.
46. Raghavan, V., *Materials Science and Engineering: A first course*. 2015: PHI Learning Pvt. Ltd.
47. Zha, S., C. Xia, and G. Meng, *Effect of Gd (Sm) doping on properties of ceria electrolyte for solid oxide fuel cells.* Journal of power sources, 2003. **115**(1): p. 44-48.